UNIVERSITY OF ALBERTA

Role of Catalytic Agents on Combustion Front Propagation in Porous Media

By

Gulcan Derya Adagulu Demirdal

©

A thesis submitted to the Faculty of Graduate Studies and Research
in partial fulfillment of the requirements for the degree of

Master of Science
in
Petroleum Engineering

Department of Civil and Environmental Engineering

Edmonton, Alberta
Spring 2007

Library and Archives Canada

Published Heritage Branch

395 Wellington Street
Ottawa ON K1A 0N4
Canada

Bibliothèque et Archives Canada

Direction du Patrimoine de l'édition

395, rue Wellington
Ottawa ON K1A 0N4
Canada

Your file Votre référence
ISBN: 978-0-494-29924-1
Our file Notre référence
ISBN: 978-0-494-29924-1

NOTICE:
The author has granted a non-exclusive license allowing Library and Archives Canada to reproduce, publish, archive, preserve, conserve, communicate to the public by telecommunication or on the Internet, loan, distribute and sell theses worldwide, for commercial or non-commercial purposes, in microform, paper, electronic and/or any other formats.

The author retains copyright ownership and moral rights in this thesis. Neither the thesis nor substantial extracts from it may be printed or otherwise reproduced without the author's permission.

AVIS:
L'auteur a accordé une licence non exclusive permettant à la Bibliothèque et Archives Canada de reproduire, publier, archiver, sauvegarder, conserver, transmettre au public par télécommunication ou par l'Internet, prêter, distribuer et vendre des thèses partout dans le monde, à des fins commerciales ou autres, sur support microforme, papier, électronique et/ou autres formats.

L'auteur conserve la propriété du droit d'auteur et des droits moraux qui protège cette thèse. Ni la thèse ni des extraits substantiels de celle-ci ne doivent être imprimés ou autrement reproduits sans son autorisation.

In compliance with the Canadian Privacy Act some supporting forms may have been removed from this thesis.

While these forms may be included in the document page count, their removal does not represent any loss of content from the thesis.

Conformément à la loi canadienne sur la protection de la vie privée, quelques formulaires secondaires ont été enlevés de cette thèse.

Bien que ces formulaires aient inclus dans la pagination, il n'y aura aucun contenu manquant.

Canada

To my husband, Barkim

ABSTRACT

Naturally occurring clays, metallic minerals and additives change morphology and surface properties of the reservoir matrix. They modify the kinetics of oxidation reactions inside the front, and promote hydrocarbon deposition. The emphasis of this work is to investigate the front performance in the presence of catalytic agents by using an analytical model. The catalytic agents are implicitly introduced to the model in terms of their effects on combustion. It is found that, while catalytic effect is more pronounced at low air injection rates, fuel deposition effect becomes significant at high air injection rates. Variations in the activation energies of the oxidation reactions are compensated by the frequency factors, and they do not have significant effect. The combustion front behavior is also analyzed in a space of parameters that includes the effects of catalytic agents. The results show that optimal reservoir conditions have the potential to enhance combustion performance.

TABLE OF CONTENTS

CHAPTER 1 INTRODUCTION 1

1.1. IN-SITU COMBUSTION PROCESSES 5

1.1.1. Dry Forward Combustion Process 7

1.1.2. Description Of Zones 8

1.2. REACTIONS OF IN-SITU COMBUSTION 9

1.2.1. Oxidation Reactions 10

1.2.2. Pyrolysis and Thermal Cracking Reactions 15

1.3. IN-SITU FUEL DEPOSITION 15

1.4. EFFECTS OF CLAYS AND METALLIC ADDITIVES ON COMBUSTION PROCESS 18

CHAPTER 2 STATEMENT OF THE PROBLEM 23

CHAPTER 3 MODELING COMBUSTION FRONT PROPAGATION 24

3.1 SINGLE-REACTION FRONT PROPAGATION 24

3.2. SEQUENTIAL REACTION COMBUSTION FRONT PROPAGATION 31

CHAPTER 4 DISCUSSION AND RESULTS 37

4.1 ADIABATIC REACTION REGIONS 37

4.2. NON-ADIABATIC REACTION REGIONS 44

4.3 COMBUSTION FRONT PROPAGATION IN THE PRESENCE OF CATALYTIC AGENTS 50

4.3.1 Catalytic Effect 50

4.3.1.1 Activation Energies 50

4.3.1.2 Frequency Factors 52

4.3.1.3 Specific Fuel Surface Areas 54

4.3.1.4 Combined Effects of the Activation Energies and Frequency Factors 54

4.3.2 Fuel Deposition Effect 56

4.3.3 Combined (Dual) Effects 61

CHAPTER 5 CONCLUSIONS AND RECOMMENDATIONS 72
REFERENCES 75
APPENDIX A 78
APPENDIX B 80

LIST OF TABLES

TABLE 1.1 - KINETIC RUNS FOR CYMRIC LIGHT CRUDE OIL (HE *ET AL.*, 2005). 21

TABLE 1.2 - KINETIC RUNS FOR CYMRIC HEAVY CRUDE OIL (HE *ET AL.*, 2005)..... 21

TABLE 3.1 - TYPICAL PARAMETER VALUES USED IN THE SINGLE-REACTION FRONT ANALYSIS (AKKUTLU AND YORTSOS, 2003)..... 28

TABLE 4.1 - INFLUENCE OF 5% CHANGE IN ACTIVATION ENERGIES ON HTO TEMPERATURE (V_f=100M/DAY)..... 51

TABLE 4.2 - INFLUENCE OF 5% CHANGE IN FREQUENCY FACTORS ON HTO TEMPERATURE (V_f=100M/DAY)..... 54

TABLE 4.3 -INFLUENCE OF 5% CHANGE IN HYDROCARBON FUEL DENSITIES ON HTO TEMPERATURE (V_f=300M/DAY)..... 56

LIST OF FIGURES

FIGURE 1.1 - IN-SITU COMBUSTION ZONES AND TEMPERATURE PROFILE (PRATS, 1982). 7

FIGURE 1.2 – (A)TGA AND (B)DSC THERMOGRAMS FOR HUNTINGTON BEACH OIL AND SAND MIXTURE (MAMORA, 1993) 12

FIGURE 1.3 – (A)TG/DTG AND (B)DSC THERMOGRAMS FOR GARZAN OIL AND SAND MIXTURE (KOK AND KARACAN, 2000) 13

FIGURE 1.4 - COMPARISON OF KINETIC TUBE EXPERIMENT WITH TWO-REACTION KINETIC MODEL (MAMORA, 1993) 17

FIGURE 1.5 - TEMPERATURE VERSUS DISTANCE. 22

FIGURE 3.1 - ADIABATIC SINGLE-REACTION FRONT VELOCITY VERSUS INJECTION VELOCITY FOR VARYING INJECTED OXIDANT CONCENTRATION (AKKUTLU AND YORTSOS, 2003) 28

FIGURE 3.2 - DEPENDENCE OF NON-ADIABATIC SINGLE-REACTION (HTO) FRONT TEMPERATURE (A) AND FRONT VELOCITY (B), ON THE INJECTION VELOCITY. (AKKUTLU AND YORTSOS, 2003) 30

FIGURE 3.3 - SCHEMATIC ILLUSTRATION OF DISCONTINUOUS HTO AND LTO REACTION REGIONS PROPAGATING COHERENTLY IN THE RESERVOIR WITH THICKNESS H. (AKKUTLU AND YORTSOS, 2004) 34

FIGURE 4.1 - PROPERTIES OF THE ADIABATIC COHERENT FRONT PROPAGATION VERSUS INJECTION VELOCITY FOR VARYING ACTIVATION ENERGY RATIO, R_E. R_Q=0.5, α=0.6, R_F=1.33 39

FIGURE 4.2 - PROPERTIES OF THE ADIABATIC COHERENT FRONT PROPAGATION VERSUS FUEL RATIO R_F FOR VARYING INJECTION VELOCITIES. R_Q=0.5, R_E=0.7 41

FIGURE 4.3 - NON-ADIABATIC TEMPERATURE PROFILES OF THE SEQUENTIAL REACTION 45

FIGURE 4.4 - PROPERTIES OF THE NON-ADIABATIC COHERENT FRONT PROPAGATION FUEL RATIO R_F FOR VARYING INJECTION VELOCITIES. R_Q=0.5, R_E=0.7. CONSTANT HEAT LOSS RATE: $\tilde{h}/H$=0.039 KW/M^3-K. 46

FIGURE 4.5 - PROPERTIES OF THE NON-ADIABATIC COHERENT FRONT PROPAGATION VERSUS INJECTION VELOCITY. R_Q=0.5, R_E=0.7, α=0.6, R_F=1.33. 49

FIGURE 4.6 - SEPARATION DISTANCE OF THE NON-ADIABATIC FRONTS VERSUS THE EXTERNAL HEAT LOSS RATE COEFFICIENT. R_Q=0.5, R_E=0.7, α=0.6, R_F=1.33..... 50

FIGURE 4.7 - CATALYTIC EFFECTS ON IN-SITU COMBUSTION PROCESS. REACTION REGION (A) TEMPERATURES, (B) PROPAGATION VELOCITY AND (C) SEPARATION DISTANCE VERSUS AIR INJECTION VELOCITY. 53

FIGURE 4.8 - HYDROCARBON DEPOSITION EFFECT ON IN-SITU COMBUSTION (CASE 9): TEMPERATURES OF THE REACTION REGIONS VERSUS AIR INJECTION VELOCITY. THE HYDROCARBON AMOUNT AHEAD OF THE LTO REGION IS TWO TIMES LARGER THAN THE BASE VALUE. 58

FIGURE 4.9 -HYDROCARBON DEPOSITION EFFECT ON IN-SITU COMBUSTION (CASE 10): TEMPERATURES OF THE REACTION REGIONS VERSUS AIR INJECTION VELOCITY. THE HYDROCARBON AMOUNT AHEAD OF THE LTO REGION IS 50% LARGER THAN THE BASE VALUE. 58

FIGURE 4.10 - HYDROCARBON DEPOSITION EFFECT ON IN-SITU COMBUSTION (CASES 9 AND 10): SEPARATION DISTANCE OF HTO AND LTO REACTION REGIONS VERSUS AIR INJECTION VELOCITY. 59

FIGURE 4.11 - DUAL EFFECT (CASE 8 + CASE 10) OF CLAYS/ADDITIVES ON FRONT PROPERTIES 59

FIGURE 4.12 - DISTRIBUTION OF THE SOLUTIONS IN THE HTO FUEL GENERATION SPACE. (X, Y) COORDINATES ARE (P^{o}_{FL}, P^{o}_{FH}), INJECTION VELOCITY IS 300 M/DAY. 66

FIGURE 4.13 - DISTRIBUTION OF THE SOLUTIONS IN THE SPACE OF DUAL EFFECTS. INJECTION VELOCITY IS 300 M/DAY..... 68

FIGURE 4.14 - COMPARISON OF THE FRONT PROPERTIES UNDER THE OPTIMAL INFLUENCE OF CATALYTIC AGENTS WITH THE BASE-STATE SOLUTION OF FIGURE 4.13..... 70

LIST OF NOMENCLATURE

a_s	=	Specific fuel surface area per unit volume, m^2/m^3
E	=	Activation energy of the reaction, kJ/kmole
h	=	Dimensionless convective heat transfer coefficient
H	=	Reservoir thickness, m
k	=	Pre-exponential factor, kW-m/atm-kmole
p	=	Initial total gas pressure in pore space, atm
Q	=	Heat of reaction, kJ/kg fuel
q	=	Total heat content of the reservoir,
R	=	Universal gas constant, kJ/kmole-K
T_f	=	Front temperature, °K
T_o	=	Initial temperature, °K
v_i	=	Injection velocity, m/day
V	=	Common velocity of the fronts, m/day
V_D	=	Nondimensional front velocity
Y_H	=	Mass fraction of the injected oxygen, kg/kg

Greek Letters

λ	=	Thermal conductivity kW/m-K
θ_f	=	Front temperature, °K
ρ^o_f	=	Initially available fuel mass density, kg/m^3
ϕ	=	Porosity, fraction
$(1-\phi)c_s\rho_s$	=	Heat capacity of solid matrix, kJ/m^3-K
α_s	=	Effective thermal diffusion coefficient, m^2/s
γ	=	Arrhenius number
μ	=	Dimensionless stoichiometric coefficient for oxygen
ξ^*	=	Dimensionless separation distance

CHAPTER 1

INTRODUCTION

Thermal recovery is the principal approach to reduce viscosity of heavy crude oil by applying heat into a subsurface oil reservoir. The necessary thermal energy can be generated at the surface and introduced into the reservoir by means of injecting steam, hot water or gas. It may also be generated in-situ (in-place) by injecting air and oxidizing heavy components of the crude oil in place. The latter approach for recovery has long been recognized and known as the air injection and in-situ combustion.

Air injection and in-situ combustion processes have several advantages when compared with the other thermal heavy oil recovery techniques. Among them, the most important one is related to instant availability and cost of the injection fluid regardless of the reservoir location. Furthermore, and perhaps even more distinctively, air injection processes bypass a necessity to minimize the wellbore-related heat losses and the accompanying injector insulation costs realized during the other thermal recovery operations. During air injection, unlike the high-temperature injection fluids, no heat losses take place until the injected air reaches the reservoir and confronts the deposited hydrocarbons. Consequently, air injection processes could perhaps be carried out in deeper reservoirs having thinner and tighter sand sections where injection of hot fluids may not be viable.

During any air injection process, propagation of a self-sustaining combustion front in the subsurface formation is, however, necessary for improved oil recoveries. It is desired to maintain a stable high-temperature combustion front that travels away

from the air injector further deep into the reservoir towards the production well(s), uniformly sweeping the in-place fluids. The fuel necessary for high-temperature oxidation reactions and the associated front self-sustainability is a carbon-rich residue resulting from a series of complex in-situ processes: low-temperature oxidations, cracking and coking (pyrolysis) reactions, in-situ generated steam-based distillation and, finally, multi-phase displacement. These sequentially take place ahead of the moving combustion front and their relative locations in the reservoir are dictated by a non-uniform temperature profile monotonously decreasing further away from the combustion front.

The produced oil is often upgraded and, hence, lighter than the original oil in place because of the in-situ consumption of the heavier fractions at the combustion front and due to processes, e.g., distillation, taking place ahead of it. Hence, the air injection processes may have an added benefit of recovering in-situ upgraded heavy oils.

Despite these potential advantages, the air injection processes have not been widely used in the field primarily due to operational and technical difficulties. It is reported that among the 1.3 million b/d of oil produced by thermal methods only 2.2 % is produced by in-situ combustion (Moritis, 1998).

One major technical difficulty that limits their practical application is related to the complex interaction of the combustion front with the preceding phenomena under the reservoir conditions. The latter take place at large reservoir scale, they are under a restrictive influence of the nonuniform temperature profile, distribution of which is dictated by the combustion front. On the other hand, the issues related to the combustion front performance, in terms of the amount of in-situ generated heat, front temperatures and propagation speeds, are closely tied to in-situ deposition and availability of the hydrocarbon fuel generated by the preceding phenomena. If the deposited fuel amount is not sufficient, as often the case with lighter oil reservoirs,

the front may propagate in an unstable combustion mode susceptible to detrimental reservoir conditions, e.g., high reservoir heat losses, and could even become extinct. To the contrary, if the deposited fuel amount is large, often the case with heavy oil reservoirs, bitumen deposits and oil shales, the front propagation velocities are expected to be significantly low which significantly slows down the operations and brings an uneconomically high air compression and injection costs for the production (Alexander *et al.*, 1962). Thus, the air injection processes depend upon not only a detailed analysis of the reservoir and fluid properties showing the existence of optimum conditions in-place but also a better understanding of the complex physical and chemical nature of the phenomena under the reservoir conditions.

A series of experimental investigations have been performed since mid 1980s mainly focusing on application of the air injection processes to a larger range of reservoirs with varying rock matrix and fluid characteristics. These investigations were involved with the optimization of the combustion front in the presence of naturally occurring clays and metallic minerals or water-soluble metallic salt additives with the potential to play a catalytic role on the combustion reactions. The results of these experimental studies have shown that the natural occurrence of clays or addition of certain metallic salts have the potential to affect the overall performance of in-situ combustion by changing the oxidation reaction kinetics and by modifying the specific surface area of the matrix for fuel deposition. However, it has not been understood how the presence of these substances affects the combustion front propagation. The latter is a question of significant importance for the design of air injection processes. The main objective of this study is, thus, investigation of the combustion front performance in the presence of catalytic agents under idealized reservoir conditions.

Understanding the effect of catalytic agents on the combustion performance requires that the mechanisms of combustion in their presence is known. Due to complex nature of the crude oil components and their numerous reactions in the presence of

oxygen under non-isothermal conditions, the task is, however, a difficult one in the laboratory or using a numerical approach. In this work, self-sustaining combustion front propagation is considered analytically using a sequential-reaction (fuel generating and fuel burning) front propagation model. Considering the complexity of problem, the approach is quite simple, although it makes rigorous analysis of the in-situ fuel generation and fuel consumption processes along with their nonlinear interactions. In essence, it builds on a recent description of the single-reaction combustion front propagation using large activation energy asymptotics (Akkutlu and Yortsos, 2003) with the purpose of understanding the combustion front behavior under detrimental reservoir conditions (i.e., these conditions that may lead the combustion to its extinction limit, such as insufficient hydrocarbon deposition and reservoir heat losses) and identifying any possible role (whether catalytic or not) the naturally occurring minerals and additives could play on the front optimization. For this, reservoir conditions under which the reaction regions travel coherently needs to be identified and their self-sustainability limits in the presence of reservoir heat losses needs to be investigated. Effects of kinetic parameter for fuel generation and combustion reactions (i.e., frequency factors, deposited hydrocarbon and generated fuel specific surface areas and activation energies) on the combustion front performance also need to be investigated. Finally, the combustion front behavior is to be analyzed in the space of parameters that are influenced by the presence of catalytic agents.

In the remaining of this chapter, air injection and in-situ combustion processes are described. Body of literature on this topic has been expanding since 1950s; consequently, it is currently vast. Therefore, the focus shall immediately be on primary method also known as the dry forward in-situ combustion. The method is also used as a prototype to introduce the preceding phenomena and to delve into the nature of combustion reactions. Following, the complex fuel deposition phenomena is discussed and the experimentally observed effects of the catalytic agents will be shown in §1.3 and §1.4, respectively.

1.1. In-Situ Combustion Processes

Dry, forward combustion is the most common form of the air injection and in situ combustion processes. In this process, air is injected into the reservoir and, following ignition downhole at the sand face, the combustion front develops, moving away from the injector towards the producer(s). Ignition may be spontaneous or it can be initiated using downhole electrical or gas igniters.

Wet combustion is a form of forward combustion method in which, water is injected into the reservoir during or after the combustion process started. During the dry forward combustion process, large amount of heat is stored in the swept zone and the adjacent formations. The injected water, having higher heat capacity than air, recovers the heat in the swept zone and carries it downstream towards the combustion front in the form of steam (Dietz and Weijdema, 1963, Beckers and Harmsen, 1970). With the re-introduction of this additional energy, more efficient oil displacement could be achieved. Gravitational forces, however, may adversely influence the wet combustion process. Having significantly larger density than the preheated air, the injected water and air could be easily segregated in the swept zone. Hence, water/air may not reach and sweep the upper/lower parts of the reservoir. In addition, excessive volumes of the injected water may accumulate in the lower parts, consequently, causing difficulties in sustainability of the combustion front.

Reverse combustion is another modification of the air injection process. The combustion reactions are initiated at the production well in this case and the combustion front moves towards the injection well against a cold air influx. Reverse combustion is applicable to highly viscous heavy oil reservoirs that have extremely low mobility. It has also been proposed for generation of high permeability channels during in-situ coal gasification (Britten and Krantz, 1986). A major disadvantage of this process is to initiate spontaneous ignition around the injector during production.

Several variants of the dry and wet in-situ combustion processes have been proposed with the purpose of improving their effectiveness under certain reservoir conditions. An example of these variants is COFCAW (Combination of forward combustion and water flooding) process which presumably requires less total volumes of air to be injected and fuel to be generated and consumed. It may result in larger amounts of recoverable oil (Parrish and Craig, 1969).

Attractive new recovery schemes appeared, in particular, along with the recent developments in horizontal well technology. These approaches integrate horizontal well technology and the concept of oil gravity drainage with the conventional air injection processes. These processes, however, are still in their infancy; although they have the potential to increase oil recovery substantially, their performances are yet to be tested under the reservoir conditions. In their simplest form, these processes similarly require continuous injection of air to a subsurface heavy oil reservoir and continuous maintenance of the combustion area between the injected fluid and in-place oil. Following an initial transition period, the combustion front develops and propagates laterally above a close by horizontal production well so that, once upgraded and mobilized ahead of the front, oil phase could readily be drained by gravity and produced. COSH (Combustion Override Split-production Horizontal-well) is one example variant that uses a horizontal production well. The air is injected through several vertical injectors located above and close to the horizontal producer (Kisman and Lau, 1993). THAI (Toe to heel air injection) is another variant of forward combustion process, in which forward in-situ combustion and advanced horizontal well concepts are integrated (Greaves and Turta, 1997). Instead of vertical producer (in conventional in-situ combustion), a horizontal producer well is placed such that the toe of the horizontal producer is located close to the injector. In the process, the combustion front propagates along the horizontal producer, from the 'toe' position, to the 'heel' (Greaves *et al.*, 1993; Greaves and Al-Shamali, 1995, 1996).

1.1.1. Dry Forward Combustion Process

In dry forward combustion process, the combustion zone is identified by a characteristic region of high temperatures. Figure 1.1 shows location of the combustion zone as the shaded area in a one-dimensional temperature profile of the dry forward combustion process. The combustion zone is narrow, dividing the reservoir into two parts: the burned (i.e., heated or swept) zone and the unburned zone. The injected air flows at rates higher than the speed of combustion zone propagation and is preheated in the burned zone. With the continuous air injection, the front progresses deep into the reservoir. Various other zones are developed ahead of the combustion zone, i.e., in the unburned zone, involving a series of displacement processes characterized by multi-component phase change and multi-phase flow phenomena. Temperature distribution and relative location of these zones formed during the dry forward combustion process are also shown in Figure 1.1.

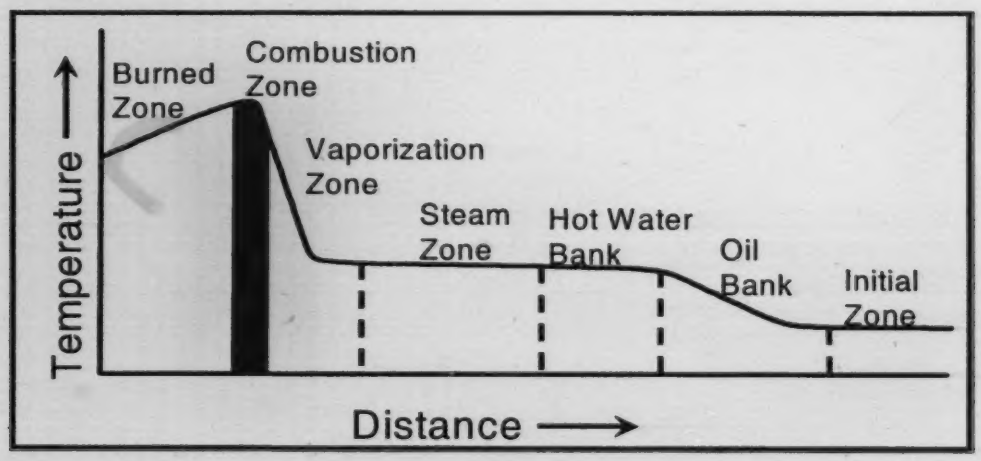

Figure 1.1 - In-situ combustion zones and temperature profile (Prats, 1982).

1.1.2. Description of Zones

Burned Zone: The burned zone is portion of the reservoir subjected to the in-situ combustion process, and therefore, it is often referred to as the swept zone. It is dominated by flow and preheating of the injected air. In this zone, mineral alteration usually occurs due to high temperatures. As shown in Figure 1.1, the temperature profile in this zone shows a monotonous decrease with the relative distance to the combustion zone location. This is due to the existence of large temperature gradients and the associated heat fluxes from the burned zone to the surrounding formations, i.e., reservoir heat losses.

Combustion Zone: It is the place where heat generation occurs due to a series of oxidation reactions taking place between the injected oxygen and in-situ generated fuel. In this zone, temperature may range between 350-650°C depending on the nature of crude oil and the quantity of fuel consumed. As the result of oxidation reactions, gaseous phase combustion products are generated, i.e., water vapor and carbon oxides. The combustion zone is often identified as a narrow moving boundary during the combustion tube experiments when its thickness is measured on the order of centimeter, typically 1-10 cm. During a field application, its thickness is estimated to be on the order of a meter.

Vaporization and Cracking Zone: Downstream end of the combustion zone, vaporization and cracking processes take place. As temperature of the local volume element ahead of the combustion zone increases, interstitial water and lighter components of the crude oil are vaporized and the remaining heavier components may undergo thermal cracking process where the temperatures exceed about 300°C. The resulting vapors are carried downstream by the filtrating gas stream and they eventually arrive at the cooler regions where they condense and mix with the original crude oil in-place. Condensing water vapor and distilled hydrocarbons may accumulate throughout the air injection process and eventually form a water bank

and an "upgraded" oil bank. Products of the cracking process are volatile hydrocarbon fraction and non-volatile heavy residue. The former may join the gas stream; as the latter may become part of the fuel consumed in the combustion zone.

Steam Zone: Steam zone is located ahead of the vaporization/cracking zone. During the air injection process, this zone develops as the result of vaporization and accumulation of the interstitial water along with the water produced inside the combustion zone. In the steam zone, temperature is around 150-250°C depending on the partial pressure of the water in the vapor phase. The steam zone temperature is nearly constant due to low partial pressure of the water in the vapor phase. In this zone, the hydrocarbons stripped in the vaporization zone may condense and dissolve in the original crude. Hence, steam zone involves simultaneous multi-phase flow of steam, oil, water, and flue gases. Depending on the temperature, the oil may also be subjected to "visbreaking" reactions in this zone resulting in reduced viscosities.

Hot Water and Oil Banks: A hot water bank is developed further downstream of the vaporization and steam zones. Local temperatures here are lower than the condensation temperature of steam. Existence of high water saturations (relative to oil and gas) characterizes this zone. The oil bank precedes the water bank and contains a liquid mixture of the displaced crude oil and the distilled hydrocarbons.

During the forward air injection processes, the displacement is primarily due to vaporization, steam and gas drive, hot water drive and miscible re-condensed light hydrocarbon drive.

1.2.Reactions of In-situ Combustion

A great deal of experimental work has been performed to understand the oxidation of crude oils, their fractions and oil/sand mixtures. Differential thermal analyses (DTA) and Thermogravimetric analysis (TGA) have extensively been used to obtain

information about the nature of oxidation reactions taking place during air injection and in-situ combustion processes.

DTA is a technique in which a crude oil and sand mixture is heated at a uniform rate while air flows through the mixture. Difference between the temperatures of a sample and reference is recorded. In TGA, a sample of crude oil and sand mixture is heated at a constant rate in the presence of flowing air. Changes in weight of the sample are recorded as a function of temperature and/or time. DSC is similar to DTA in operation and is used to determine the heat of reaction (enthalpy) and to delineate different reaction regimes. In DSC the energy released or absorbed via chemical reaction is monitored during the heating process.

Previous experimental works showed that the overall reaction mechanism of crude oils in porous media is due to an overlap of several oxidation reactions that occur at different temperature ranges. On the thermograms, these have been classified as the regions of low-temperature, medium-temperature and high-temperature oxidation reactions. In the absence of oxygen, there also exist pyrolysis and thermal cracking reactions during the in-situ combustion processes.

1.2.1. Oxidation Reactions

Low-temperature oxidation (LTO) reaction region is often considered as the region where small and weak chains of hydrocarbons are oxidized yielding water and partially oxygenated hydrocarbons such as carboxylic acids, aldehydes, ketones, alcohols, and hydroperoxides. In the middle-temperature oxidation (MTO) region, the products of LTO are converted to heavier hydrocarbons to be consumed in the main combustion region. High-temperature oxidation (HTO) region is the main combustion region where fuel is oxidized with the incoming oxygen, generating CO_2, CO, and water (Burger and Sahuquet, 1972).

Figure 1.2, and Figure 1.3 show thermograms for two different types of crude oils. Figure 1.2 shows TGA and DSC thermogram for the first oil sample, Huntington Beach, (Mamora, 1993). On the TGA thermogram, three temperature regions are indicated by the rate of decrease in weight with temperature measurements. A sharp rate of decrease was observed in the temperature range, 27°-280°C, due to vaporization of the light hydrocarbon fractions. DSC thermogram shows vaporization as a slightly endothermic reaction indicating that heat is removed from the system due to vaporization. The region of vaporization shows itself with a hump trace in DTG and a rapid weight loss in the TGA curves. In the range of 280-400°C, a slight rate of decrease in weight was found, which is indicated as the first exothermic reaction by the DSC thermogram. At higher temperatures, in the range of 400-500°C, the rate of weight decrease becomes very sharp due to rapid oxidation of the hydrocarbons, which corresponds to a highly exothermic reaction on the DSC thermogram. The two temperature peaks on the DSC thermograms are related to the presence of LTO and HTO reactions.

In Figure 1.3, on the other hand, four different temperature regions are observed for the second crude oil sample, Garzan (Kok and Karacan, 2000). Similarly, in between the temperature range, 25-300°C, vaporization region appears which is slightly endothermic. Low-temperature oxidation occurs in the 300 to 377°C temperature range. There exists a slight rate of decrease in weight in this range and DSC diagram showing the existence of an exothermic reaction. The MTO temperature interval is also indicated as exothermic reaction on DSC thermogram, between 377- 467°C. Whereas HTO, the main combustion region, occurs in the between 490-580°C. This region shows itself as a steep rise in the DTG curves, and it is observed as a highly exothermic reaction on the DSC thermogram.

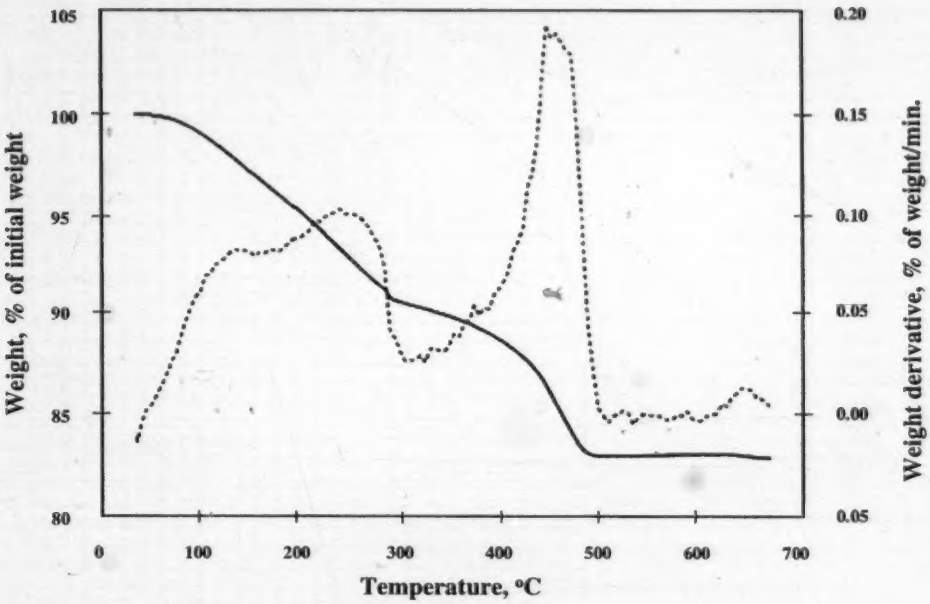

(a)

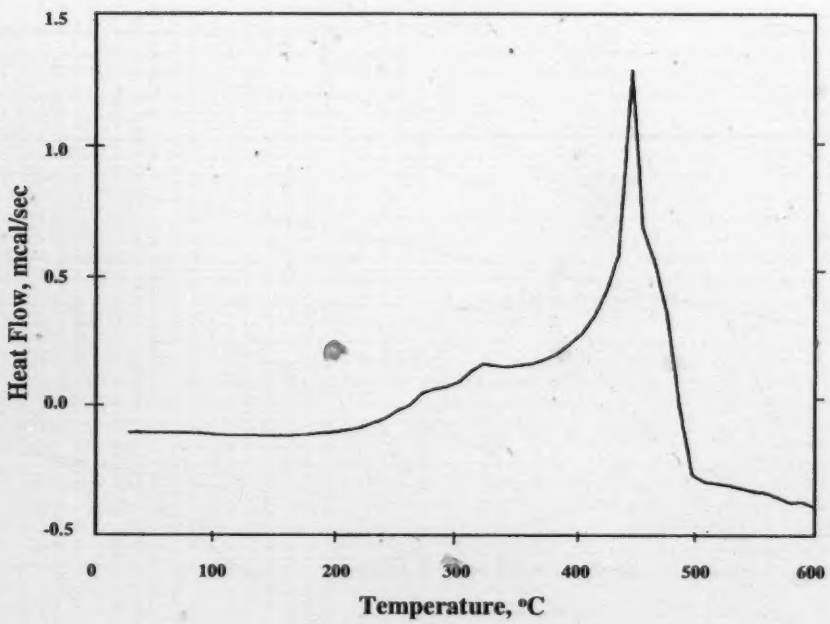

(b)

Figure 1.2 –TGA (a) and DSC (b) Thermograms for Huntington Beach Oil and Sand Mixture (Mamora, 1993)

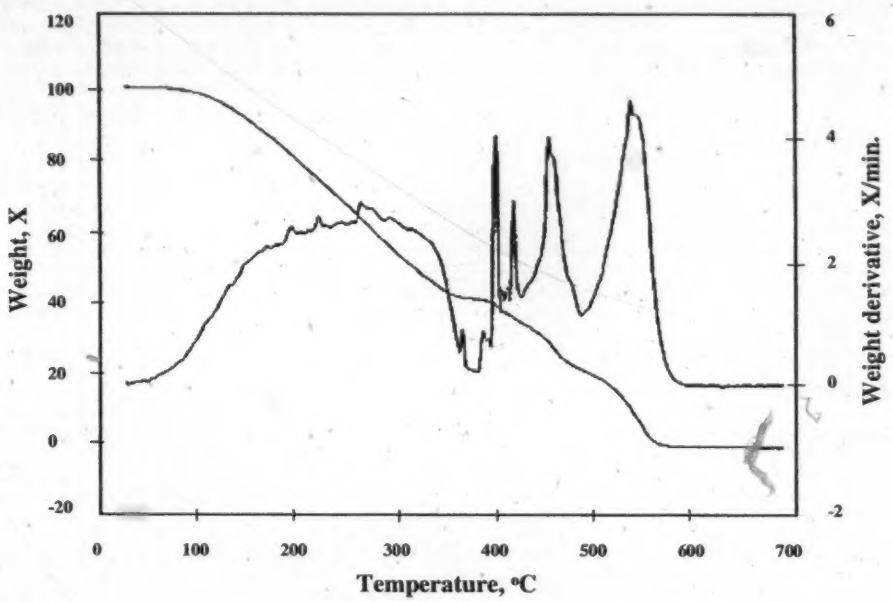

(a)

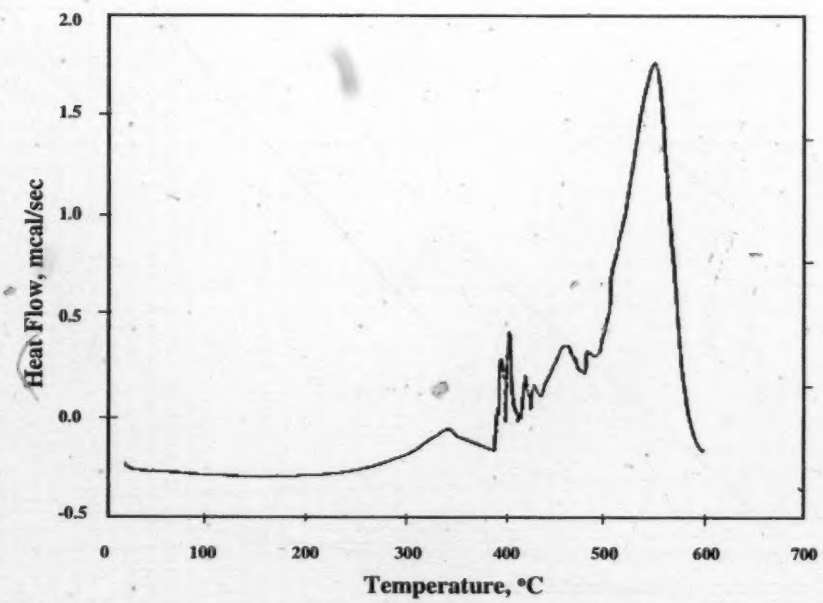

(b)

Figure 1.3 –TG/DTG (a)and DSC (b) Thermograms for Garzan Oil and Sand Mixture (Kok and Karacan, 2000)

There exist numerous other experimental studies in the literature repeatedly showing the appearance of LTO and HTO reaction regions on the thermograms for various types of crude oil and sand mixtures.

Low-temperature (LTO) reactions

Low-temperature oxidation reactions are highly complex and hence poorly understood. These reactions take place when the injected oxygen bypasses or when the excess (unreacted) oxygen leaks through the HTO reaction region, reaching and having contact with the deposited heavy hydrocarbon components. The former is more pronounced with the reservoir heterogeneity. They are characterized by relatively small amounts of carbon oxides production. The LTO reactions take place at temperatures less than 350°C, and yields water and partially oxygenated hydrocarbons such as carboxylic acids, aldehydes, ketones, alcohols, and hydroperoxides (Burger and Sahuquet, 1972).

Alexander et al (1962) studied the factors affecting the HTO fuel availability by carrying out effluent gas analysis experiments. In their work, a sample of oil and sand mixture is subjected to continuous injection of air and a heating schedule. The results showed that the deposition of coke-like residues on the sand grains is promoted by the LTO reactions. They also observed that when the temperature is decreased, more fuel is generated due to increasing LTO reactions.

(Dabbous and Fulton, 1974) showed that light crude oils could become more susceptible to LTO than the heavy oils, and the LTO reactions may change the fuel characteristics and coked sand properties during the air injection process.

High-temperature (HTO) reactions

The high temperature oxidation (HTO) region is the main combustion area where heterogeneous H/C bond scission reactions occur between oxygen and a semi-solid fuel, producing water and carbon oxides. HTO reactions are heterogeneous reactions,

i.e., gas-solid and gas-liquid residue reactions, and the stoichiometry of an HTO reaction is often given by (Behnam and Poettmann,1958) :

$$CH_n + \left[1 - \frac{m}{2} + \frac{n}{4}\right] O_2 \rightarrow [1-m]CO_2 + mCO + \frac{n}{2} H_2O$$

where n = atomic ratio of hydrogen to carbon and m = fraction of carbon oxidized to CO. In the case of heavy crude oils and bitumen, the generated heat of combustion is sufficiently high for the HTO reactions to dominate the front propagation in reservoir and, ultimately, oil recovery.

1.2.2. Pyrolysis and Thermal Cracking Reactions

Pyrolysis reactions are formally defined as chemical decomposition of the organic materials by heating in the absence of oxygen. Pyrolysis is often considered as reaction endothermic in nature and defined as

$$(C_x H_y) \rightarrow xC \downarrow + \frac{y}{2} H_2$$

Thermal cracking, on the other hand, is the process of breaking down larger molecules of hydrocarbons in the presence of heat. It is often defined as,

$$(C_x H_y) \rightarrow C_n H_m \downarrow + C_{x-n} H_{y-n}$$

1.3. In-situ Fuel Deposition

Fuel deposition refers to pore-scale mechanisms of fuel generation in the reservoir rock matrix during the air injection and in-situ combustion processes. The quantity of

fuel deposited is an important consideration because its reaction by the injected oxygen and its consequent consumption could influence the combustion front propagation. When the concentration of deposited fuel is too low in the matrix, the heat generated by the oxidation reactions may not be enough for the frontal self-sustainability; on the other hand, when the fuel concentration is too high, in order to consume larger quantities of fuel, the front may propagate slower and oxygen needed for the in-situ combustion process may become uneconomically high.

The mechanisms of fuel deposition have been investigated by several authors. Alexander *et al.* (1962) investigated the factors that affect fuel availability by performing experiments based on the effluent gas analysis. They observed that the fuel concentration increases with initial oil saturation, oil viscosity and Conradson residue (ASTM), and decreases with the increasing atomic H/C ratio and the oil API gravity. Similar results were also found by Showalter (1963). Alexander *et al.* (1962) also indicated that the LTO reactions could have pronounced effect on the amount of fuel deposition. Furthermore, for the first time, they mentioned a possibility of propagating LTO reaction region ahead of the HTO during an in-situ combustion process.

Based on the thermogravimetric experiments, Bae (1977) showed that crude oil oxidation generally starts at a higher temperature and less heat is generated with decreasing pressure. In Bae's work, distillation is suggested as the governing mechanism for deposition of fuel. Accordingly, with the increasing reservoir pressures, distillation performance of the air injection process decrease and, hence, more fuel is likely to be generated.

Poettmann *et al.* (1967) showed that the specific grain surface area of the reservoir matrix has a direct effect on fuel deposition. Later, Vossoughi *et al.* (1982) argued that the amount of fuel deposited increases in the presence of clay particles in the reservoir matrix.

Moore et al (1986) carried out experimental study and compared the effects of thermal cracking and LTO reactions on fuel deposition during an in-situ combustion process. Their results showed that the LTO reactions could cause significant compositional changes at relatively short time spans; whereas, significantly higher temperatures and longer times are required for thermal cracking.

Mamora (1993) considered the experimental occurrence of LTO and HTO reactions during a series of kinetic tube experiments and concluded that the LTO reactions are mainly responsible for fuel generation. Based on this premise, he developed a two-reaction hydrocarbon oxidation kinetic model, Figure 1.4.

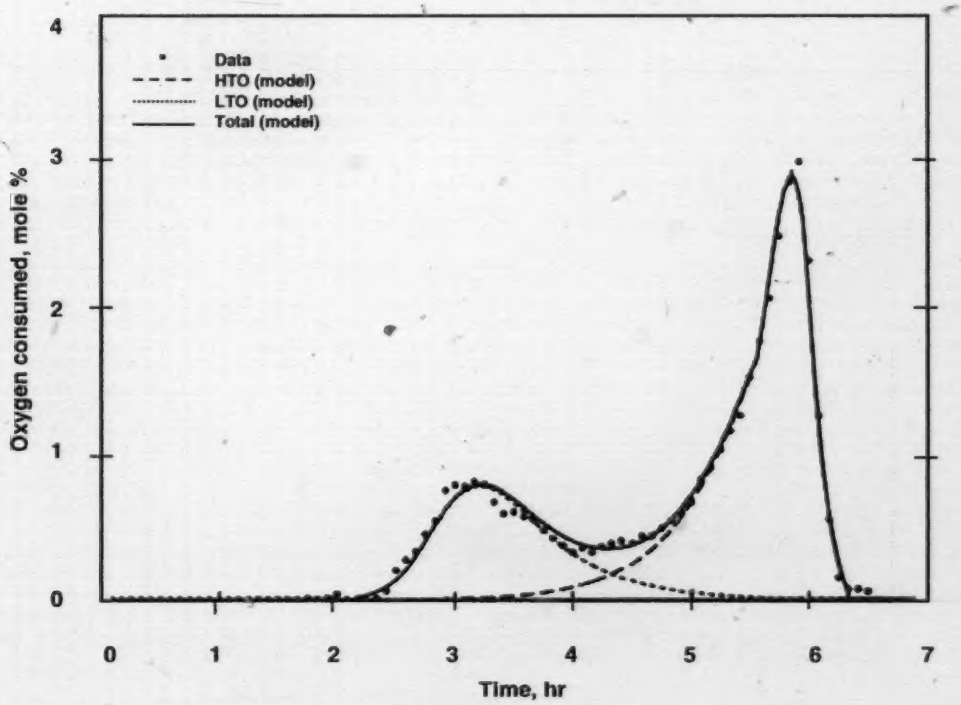

Figure 1.4 - Comparison of kinetic tube experiment with two-reaction kinetic model (Mamora, 1993)

1.4. Effects of Clays and Metallic Additives on Combustion Process

Catalyst is a substance that modifies and increases the rate of a chemical reaction without being consumed in the process. In chemical industry, metals have been known for their catalytic ability in hydrocarbon oxidation and cracking reactions. Many studies appeared in the literature investigating the effects of metallic additives on the oxidation characteristics of crude oils.

Burger and Sahuquet (1972) performed kinetic experiments and observed that the oxidation reactions could occur at lower temperatures and the area under the high temperature peak increases in the presence of additives. He interpreted the former observation due to an increase in oxidation reaction rate and the latter due to an increase in the deposited fuel amount.

Fassihi (1981) run kinetic experiments by using 27°API oil. He compared the effluent gas data for the clean sand with the one added copper. The results showed that the activation energy of HTO reaction region decreases about 50 percent and activation energy of MTO reaction region increases about 50 percent. No significant change is observed in the LTO reaction region other than a higher Arrhenius constant.

Vossoughi *et al.* (1982) studied effects of clays on the in-situ combustion process. The combustion tube experiments showed that in the presence of clays the heat of combustion per unit volume of sand increased leading to higher peak combustion temperatures. They interpreted these results as the influence clay on the fuel deposition. Accordingly, having larger surface area with respect to the sands, clays create an environment locally promoting fuel deposition in the matrix. In addition, they investigated variations on the kinetics of the oxidation reactions due to the presence of clays using TGA and DSC thermograms. Their experimental study combines four adiabatic dry combustion runs in which, sand mixtures of varying

kaolinite content are saturated with crude oil and water. They also used amorphous silica powder in the sand mixture on the fourth run to compare the results with clay results. They observed that the addition of kaolinite and of silica powder to crude oil changed significantly the shapes of TGA/DSC thermograms indicating catalytic effects on the reactions in terms of their activation energies.

Drici and Vossoughi (1985) studied the effects of metal oxides on combustion characteristics of the crude oil by using DSC and TGA analysis. The results showed that as the metal oxides concentration increases the amount of heat released in the LTO reaction region gradually increases. The combustion peak temperature shifts to a lower temperature and became smaller and smoother which reflects a more homogeneous composition of the solid residue. They also noted that, when the catalytic effects are investigated, the change in the reaction rate constant must be considered simultaneously with the activation energy of reaction.

De los Rios *et al.* (1988) and Shallcross *et al.* (1989) performed kinetic experiments with various metallic additives and developed an analytical model to estimate the kinetic parameters of the oxidation reaction regions, namely LTO, MTO and HTO. They found that iron and tin salts enhance fuel deposition and increase oxygen consumption while copper, nickel, and cadmium salts show no apparent effect. For each oxidation reaction, the activation energies are estimated using their model. For most of the catalytic agents, their results showed that the activation energy of HTO and MTO reactions increases while that of the LTO reaction decreases.

Castanier *et al.*, (1992) carried out thirteen combustion tube runs with metallic additives. In the experiments, four different types of oil were used. The results showed that tin, iron and zinc enhances the combustion efficiency, while copper, nickel and cadmium have little or no effect. Increase in the fuel deposition, oxygen utilization efficiency, and front velocity are found in the presence of the former metals. In addition, zinc is found to be less effective compared to tin and iron. For

the light oil case, they observed a sustained combustion by using iron additive while combustion failed without any additive.

Holt (1992) used iron nitrate and zinc nitrate on Cymric field light and heavy oil and observed a catalytic effect of the additives. For the Cymric heavy oil, results of the kinetic experiments showed that addition of 1% iron nitrate increased fuel concentration by 20% compared to control run. On the other hand, 1% zinc nitrate increased fuel concentration by only 5%. It is noted that the generated fuels require different amounts of air to burn unit masses. They also repeated the same runs for the Cymric light oil without any additives. Sustained combustion could not be achieved, however, due to lack of fuel deposition. On the other hand, they observed efficient combustion with addition 1% (mole) iron nitrate solution.

He *et al.* (2005) explored the effect of metallic additives on in-situ combustion using combustion tube and kinetics cell. It is known that metallic additives enhance oxidation and cracking of hydrocarbons and affect the nature and amount of fuel deposited. In their paper an experimental study combining tube runs and temperature oxidation tests are described. In addition to Cymric light crude oil, Cymric heavy oil is also used during the experiments. For the tests sand, silica powder or kaolinite are mixed with water and oil. In the cases of test with metallic additive, 0.5 g of the additive is added to the water. The results of the experiments are given in their Table 1.1 and Table 1.2. It is observed that the additive improves performance in all cases including changing activation energies, greater oxygen consumption low temperature threshold and more complete oxidation. For Cymric light crude oil, the catalytic effect is obvious in the LTO where fuel deposition is increased to sustain combustion. For Cymric heavy crude oil, metallic additives are found to have effect on HTO. Kaolinite, even without metallic additive, also has an effect on crude oil combustion. They also examined sand and clay surfaces with scanning electron microscopy to evaluate any textural or compositional changes in the sand-clay mixture upon addition of metallic additive. It is observed that introduction of

metallic ions has not changed remarkably the morphology of the clay within mixtures of sand and clay. Figure 1.5 shows the temperature profile for one of the runs in their experiment. It is observed that the combustion front temperature remains around 400-450°C only for the first half of the tube which includes water with metallic additives. After passing the additive-no additive interface of the sample the front temperature started to decrease and eventually died out.

Table 1.1 - Kinetic runs for Cymric light crude oil (He *et al.*, 2005).

Kaolitine or Silica	Additive	Peak T, LTO, °C	Peak T, HTO, °C	E/R, LTO	E/R, HTO	Max O_2 LTO, %	Max O_2 HTO, %
Kaolitine	None	275	385	9647	10669	3	2.8
Kaolitine	Fe^{3+}	275	355	8535	11522	5.1	3.8
Silica powder	None	287	410	8331	10681	2.4	2.6
Silica powder	Fe^{3+}	280	370	7886	9775	2.9	2.7

Table 1.2 - Kinetic runs for Cymric heavy crude oil (He *et al.*, 2005).

Kaolitine or Silica	Additive	Peak T, LTO, °C	Peak T, HTO, °C	E/R, LTO	E/R, HTO	Max O_2 LTO, %	Max O_2 HTO, %
Kaolitine	None	270	395	9090	12319	12.6	12.2
Kaolitine	Fe^{3+}	280	355	9085	9427	13.7	18.7
Silica powder	None	265	410	7293	10489	6.3	18.4
Silica powder	Fe^{3+}	260	380	7098	10640	7	18.4

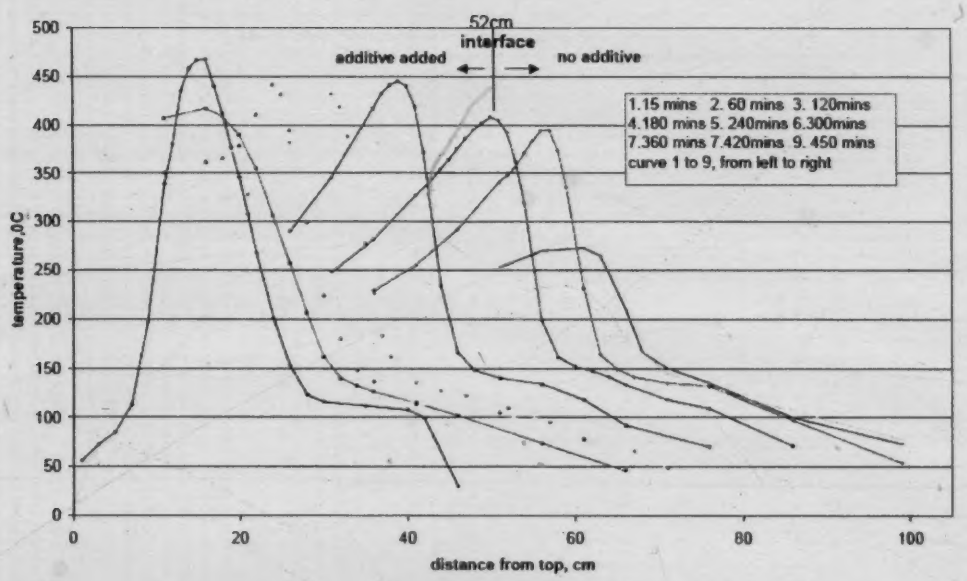

Figure 1.5 - Temperature versus distance showing the influence of additive on the combustion front propagation (He *et al.*, 2005).

CHAPTER 2

STATEMENT OF THE PROBLEM

Sustained propagation of a combustion front is necessary for improved recovery of oil during an air injection and in-situ combustion process. The front is a sharp moving boundary layer and involves the added complexities of combustion reactions. In this study, role of catalytic agents on the combustion front propagation is investigated analytically using a front propagation model involving two sequential oxidation reactions: a (high-temperature) fuel-burning reaction and a (low-temperature) fuel-generating reaction. The objectives of this study can be summarized as follows.

In the absence of catalytic agents:

1. To show the existence of sequential reaction regions propagating coherently in a homogeneous porous medium under typical reservoir conditions;
2. To investigate the interactions between the reaction regions during their coherent propagation in porous media;
3. To delineate the effects of fuel generation and combustion kinetics on the propagation.

In the presence of catalytic agents:

4. To investigate the combustion front performance under varying reservoir conditions;
5. To analyze the existence of optimal reservoir conditions, which leads to frontal coherence and has the potential to significantly enhance the air injection process.

CHAPTER 3

MODELING COMBUSTION FRONT PROPAGATION

3.1 Single-reaction Front Propagation

Consider injection of an oxidant gas into a homogeneous porous medium containing *ab initio* fuel and the resulting uniform propagation of a planar HTO front. The injected oxidant having much higher velocity than the front reaches the front and reacts with the available fuel, completely consumes it. Unreacted, excess oxygen leaks through the combustion front along with some produced gases. The front is a sink for the two reactants and a source of heat due to the exothermic nature of the reaction.

An analytical solution of the problem is possible using large activation energy asymptotics, a technique widely used in the analysis of flames, Williams, (1985). The reaction region is considered as a place of discontinuities in the appropriate variables, which include, for example, heat and mass fluxes. Jump conditions relating the changes in these variables across the reaction region are derived. The problem, then, reduces to modeling of the dynamics of a reaction front, on either side of which transport of momentum (fluids), heat and mass, but not chemical reaction, must be considered. By locally analyzing the leading-order asymptotic behavior inside the reaction region, the front velocity can also be determined in terms of the reaction kinetics. The two outside regions are coupled using the jump conditions.

Under adiabatic conditions, Akkutlu and Yortsos (2003) predicted that a sustained front propagation always exists, with the (non-dimensional) front temperature θ_f given by

$$\theta_f \equiv \frac{T_f}{T_o} = 1 - \frac{qV_D}{a(\rho v)^+ - V_D} \cong 1 + q, \tag{1}$$

where $q = \dfrac{Q\rho_f^o}{(1-\phi)c_s\rho_s T_o}$ representing the total heat content of the combustion process in the reservoir and $a = \dfrac{c_g\rho_g}{(1-\phi)c_s\rho_s T_o}$ the volumetric heat capacity of the gas with respect to that of the solid matrix. In equation (1) T is the absolute front temperature, with the sub letters f and o referring to the front and initial reservoir condition, respectively; $V_D = V/v_i$ is the dimensionless front velocity normalized with the injection velocity v_i; and $(\rho v)^+$ refers to dimensionless total gas mass flux ahead of the combustion front, which implicitly includes the reaction-generated gas mass. Also introduced above are the heat of reaction, Q, the initially available fuel mass density (per total volume), ρ_f^o. Due to small values of the volumetric heat capacity of the gas with respect to the rock, $a << 1$ is taken, hence, the right-hand side of equation (1) reduces to the thermodynamic limit $1+q$, suggesting that the front temperature could practically become independent of the front velocity V_D. Accordingly, the front temperature is higher than the initial reservoir temperature by an amount proportional to the total heat content of the reservior.

In the presence of external reservoir heat losses, description of the temperature of a (non-adiabatic) combustion front takes a different form:

$$\theta_f = 1 + \frac{q}{\Delta_h} \tag{2}$$

where $\Delta_h = \sqrt{1+4h/V_D^2}$, $h = \tilde{h}t^* /[(1-\phi)c_s\rho_s H]$ with $t^*=l^*/v_i$, ($l^*=\alpha_s/v_i$) denoting a characteristic time (space) in terms of effective thermal diffusion coefficient of the medium $\alpha_s = \lambda/(1-\phi)c_s\rho_s$. In the above, external heat losses were accounted by introducing in the total energy balance a volumetric sink term equal to $\tilde{h}(\tilde{T}-T_o)/H$. Here, $\tilde{T}$ is the absolute temperature at a given point and $\tilde{h}$ is a lumped convective-type coefficient controlling the heat transfer rate from the reservoir with a thickness H to the surroundings. As shown in equation (2), unlike the adiabatic case, the non-adiabatic front temperature depends on the front velocity V_D.

The front velocity to leading-order in the asymptotics is given by the following expression,

$$V_D^2 = \dot{A}\theta_f Y_H \exp\left(-\frac{\gamma}{\theta_f}\right) \tag{3}$$

which is valid under both adiabatic and non-adiabatic conditions. In the above, $\gamma=E/RT_o$ is the Arrhenius number, E denotes the activation energy of the reaction and R is the universal gas constant. The dimensionless parameter $\dot{A}$ reflects a combination of physicochemical properties, including the kinetics and pressure of reaction, the mass fraction of the injected oxygen Y_i and the injection velocity

$$\dot{A} = \frac{a_s\alpha_s kpY_i}{qEI_\eta v_i^2} \tag{4}$$

a_s is a function of the porosity ϕ and represents the specific fuel surface area per unit volume, k is the pre-exponential factor, p the initial total gas pressure in pore space, while the constant I_η can be taken equal to unity, without loss.

The final expression of interest is the mass fraction of the oxidant that leaves the front unreacted. This quantity is equal to

$$Y_H = \left(\frac{1 - \mu V_D}{1 + \mu_g V_D} \right). \tag{5}$$

where μ and $\mu_g = \mu_{gp} - \mu$ are non-dimensional stoichiometric coefficients for oxidant and net produced gas due to reaction, respectively, defined in terms of the mass-weighted reaction stoichiometric coefficients $\tilde{\mu}$ and $\tilde{\mu}_g$ as

$$\mu = \frac{\tilde{\mu} \rho_f^0}{\rho_{gi} Y_i} \quad \text{and} \quad \mu_g = \frac{\tilde{\mu}_g \rho_f^0}{\rho_{gi}}.$$

Details on the formulation of the governing equations, scaling, non-dimensionalization and the large-time asymptotic solutions are given in the study by Akkutlu and Yortsos (2003). In the single-reaction problem, Y_L corresponds to conditions ahead of the (HTO) front. Equation (5) shows that the excess oxygen mass fraction in the gas also depends on the front velocity and stoichiometric coefficients of the reaction. The problem becomes stoichiometrically-controlled when $Y_H = 0$, in which case the dimensionless front velocity is constant and equal to $1/\mu$. Equations (3)-(5) also apply in the case of sequential reactions. However, in that case, Y_H, being the excess oxygen fraction leaving the HTO reaction, it will become the inlet oxygen fraction for the upstream LTO reaction.

In the adiabatic case, there exists always a unique solution for the front velocity given by equation (3). This relation is plotted in Figure 3.1 as a function of the air injection velocity in a range typically used in the laboratory for investigations. Typical parameters are given in Table 3.1. It yields two limits of the solution. When the parameter Á is large (e.g., at small injection velocities) stoichiometric control

limit is reached, where the front propagation velocity becomes independent of temperature: $V_D=1/\mu$ (or in terms of dimensional velocities $V=v_i/\mu$). Hence, at this limit, the dimensional front velocity appears as directly proportional to

Table 3.1 - Typical parameter values used in the single-reaction front analysis (Akkutlu and Yortsos, 2003)

Parameter	Value
ρ^*_{fH}	19.0 kg/m^3
E_H	7.35*10E+4 kJ/kmole
Q_H	3.95E+4 kJ/kg fuel
T_o	373.15 K
p	1.0 atm
Y_i	1.0 kg/kg
v_i	100.0 m/day
R	8.314 kJ/kmole-K
k	227 kW-m/atm-kmole
a_s	1.41*10+5 m^2/m^3
λ	8.654*10E-4 kW/m-K
$c_g\rho_{gi}$	1.2338 kJ/m^3-K
$(1-\phi)\, c_s\rho_s$	2.012*10E+3 kJ/m^3-K
H	2 m
$\tilde{h}$	0.078 kW/m^2-K
$\tilde{\mu}$	3.018
$\tilde{\mu}_g$	1.0

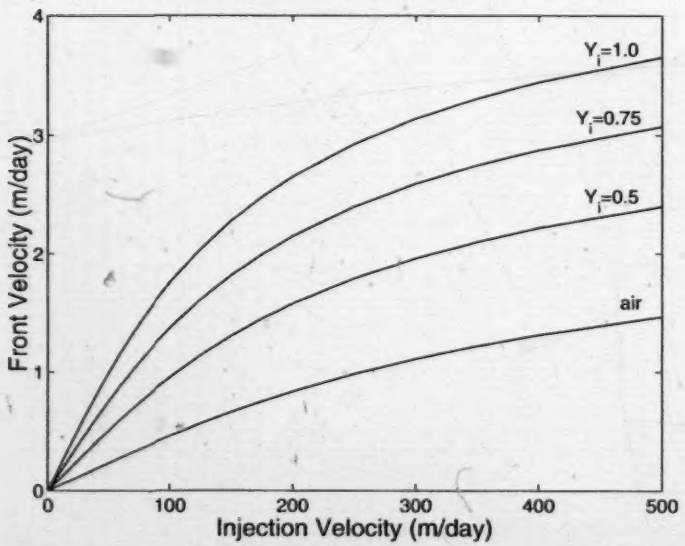

Figure 3.1 - Adiabatic single-reaction front velocity versus injection velocity for varying injected oxidant concentration (mass fraction) Y_H (denoted in the figure as Y_i). (Akkutlu and Yortsos, 2003)

the injection velocity on Figure 3.1. Also, note that its rate of change is influenced by μ which is a function of the injected oxygen concentration. When À is small, there another limit, i.e., kinetic control limit is reached. In this limit, the front velocity is influenced by the front temperature and it becomes independent of the injection velocity: V_D= À θ_f exp(-γ /θ_f). In Figure 3.1, the kinetic control limit appears as deviations from the linearity.

In the non-adiabatic case, the coupling between the combustion front propagation speed V and temperature T_f has significant implications on the propagation. The dependence of the front temperature and its velocity on the air injection rate for varying heat loss rates ($\tilde{h}$ /H) is shown in Figures 3.2a and 3.2b respectively. For sufficiently large heat loss rates, the system shows multiple steady states and extinction solutions: (1) a stable low-temperature branch near the initial condition T_o; (2) a stable high temperature branch, where rigorous combustion takes place; and (3) an unstable intermediate branch connecting the former ones. The upper branch, with high front temperature and velocities, is the solution corresponding to proper in-situ combustion front propagation. Interestingly, at higher injection velocities this branch runs parallel to the adiabatic value, although it practically never reaches it (see Figure 3.2a and compare Figure 3.1 and 3.2b). In the presence of external heat losses, the fronts propagate slower and with lower temperatures. As the heat loss rates increase, the front temperature and velocity at the extinction threshold E_c increases, namely it requires an increasingly larger injection velocity for the combustion reaction to be sustained.

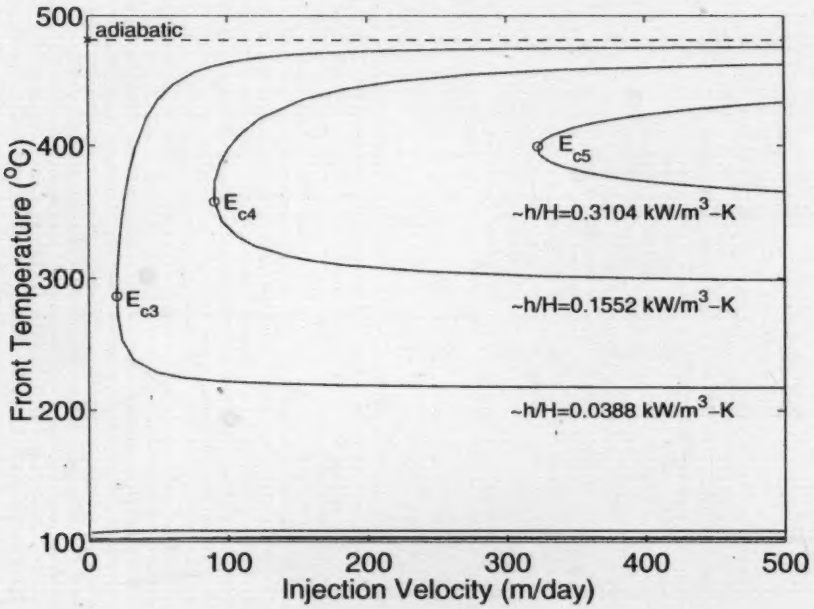

(a)

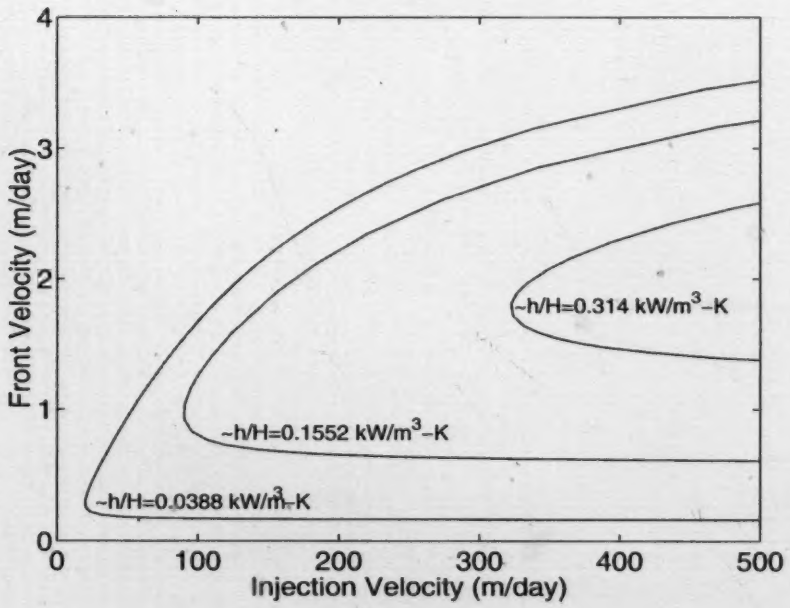

(b)

Figure 3.2 - Dependence of non-adiabatic single-reaction (HTO) front temperature (a) and front velocity (b), on the injection velocity. (Akkutlu and Yortsos, 2003)

Consider, now, propagation of the same HTO front, but in the presence of a preceding LTO reaction. The latter is also considered to involve an exothermic reaction, but with a different (less) activation energy and heat of reaction, hence, with lower front temperatures. The LTO reaction will have two effects on the combustion system: it may locally provide a preheating effect, i.e., increase the local temperature ahead of the HTO region; and it will generate the fuel necessary for the HTO reaction. The latter effect is most important, as it relaxes the previous assumption of a*b initio* fuel in the reservoir. In order to investigate the effect, however, the asymptotic single-reaction front analysis of Akkutlu and Yortsos (2003) needs to be extended. For this, we shall assume that the HTO fuel is generated at the rates and in proportion to the amount of the LTO fuel consumed. Thus, the ratio of the two initially available fuel mass densities at the HTO and LTO regions, $R_F=\rho^o_{fL}/\rho^o_{fH}$, is basically an effective stoichiometric coefficient for the LTO reaction, and will be an important parameter for consideration during the investigation, as it reflects the fuel generation efficiency of the LTO reaction.

3.2. Sequential Reaction Combustion Front Propagation

In the presence of fuel-generating and -burning reactions, the two reaction regions, an LTO downstream and an HTO upstream exist. The LTO reaction region proceeds at the rates dictated by the unburned oxygen that leaves the HTO region, and acts as the oxidant for the LTO reaction. Thus, the two regions are chemically coupled. The fronts must either travel separately, with the LTO front progressively distancing away from the HTO front, or reach a state of coherence, in which the two front velocities are the same and separated by a finite and fixed distance. The coherence conditions are obviously important and need to be investigated under the two reservoir conditions, i.e., adiabatic (closed system) and non-adiabatic (open system). In the first case, even though the fronts are separated, the HTO reaction occurs in a preheated environment. In the second, the heat losses to the surroundings dissipate

the generated heat and the only coupling between the fronts is chemical, as is also with the adiabatic case. In either case, important questions are how their interaction influences the combustion process at the reservoir scale, and whether or not this interaction is detrimental or beneficial for the in-situ combustion process.

Consider coupled reaction regions, which travel coherently with the same velocity, V_D in the reservoir. The regions are separated from each other by the distance ξ^* as shown in Figure 3.3. Because of the non-adiabatic nature of the reservoir system, the non-dimensional energy balance describing heat transfer across the combustion zone reads as follows

$$A\frac{d\theta}{d\xi}=\frac{d^2\theta}{d\xi^2}-h(\theta-1), \tag{6}$$

Here, $\xi=x-V_Dt$ is the moving coordinate with respect to the HTO reaction region, dimensionless spatial variable $x=\tilde{x}/l^*$ and $A=a\rho v-V_D\cong -V_D$ are used. The general solution of equation (6) is

$$\theta=1+ae^{r_1\xi}+be^{r_2\xi}, \tag{7}$$

where roots of its characteristic equation are as follows

$$r_1=\frac{1}{2}\left(A+\sqrt{A^2+4h}\right)>0 \quad \text{and} \quad r_2=\frac{1}{2}\left(A-\sqrt{A^2+4h}\right)<0.$$

Due to the nature of the problem, three regions are identified (Figure 3.3). Without loss, the HTO region can be assumed at $\xi=0$. Using the far-field conditions $\theta=1$ as $\xi\to\pm\infty$ and $\theta=\theta_H$ at $\xi=0$, the following general solutions in the respective regions are obtained

Region I:

$$\theta = 1 + (\theta_{fH} - 1)e^{r_1 \xi},$$

Region II:

$$\theta = 1 + c_1 e^{r_1 \xi} + c_2 e^{r_2 \xi},$$

Region III:

$$\theta = 1 + c_3 e^{r_2 \xi}.$$

To complete the problem will require formulating jump conditions across the HTO and LTO reaction regions. The jump conditions are in agreement with the single-reaction analysis of Akkutlu and Yortsos (2003) and written as follows:

$$\xi = 0 \quad : \quad [\theta]_{\xi=0^-}^{\xi=0^+} = 0, \qquad [\theta']_{\xi=0^-}^{\xi=0^+} = -q_H V_{DH} \tag{8}$$

$$\xi = \xi^* \quad : \quad [\theta]_{\xi=\xi^{*-}}^{\xi=\xi^{*+}} = 0, \qquad [\theta']_{\xi=\xi^{*-}}^{\xi=\xi^{*+}} = -q_L V_{DL} \tag{9}$$

Note that the temperature is continuous across the reaction regions, its gradients, on the other hand, contain jumps across the regions equal to the product of heat content and the propagation speed. Frontal coherence will require that the reaction regions travel with the same speed ($V_{DH} = V_{DL}$). This common velocity and the distance ξ^* between them must be determined. The system of equations has six unknowns: 3 integration constants, and θ_{fH}, V_D and ξ^*; the six equations required for the solution consists of the 4 given jump conditions and application of the front propagation velocity equation twice for each reaction region, i.e., equations 8 and 9

$$V_{DH}^2 = \dot{A}_H Y_H \theta_{fH} \exp\left(-\frac{\gamma_H}{\theta_{fH}}\right), \tag{10}$$

$$V_{DL}^2 = \dot{A}_L Y_L \theta_{fL} \exp\left(-\frac{\gamma_L}{\theta_{fL}}\right), \tag{11}$$

where the dimensionless coefficients are slightly different and given in the next page. Akkutlu and Yortsos (2004) recently presented solutions to the combustion front propagation with the sequential reaction regions using explicit formulations for the HTO and LTO front temperatures θ_{fH} and θ_{fL} which are coupled by equations (10 and 11). Our approach is different in that it enables us to obtain the complete temperature profile of the problem in addition to the common propagation speed and separation distance by using the jump conditions (8,9) and front velocity equations (10,11). Throughout the analysis, the results are often compared with their approach.

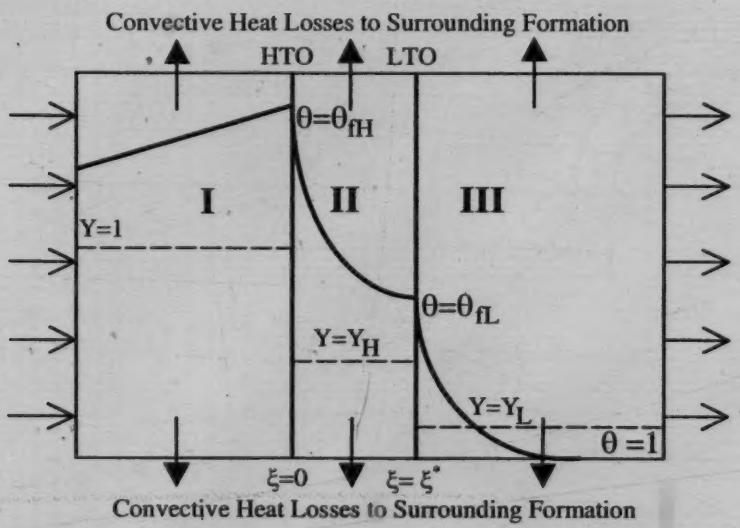

Figure 3.3 - Schematic illustration of discontinuous HTO and LTO reaction regions propagating coherently in the reservoir with thickness *H*. (Akkutlu and Yortsos, 2004)

$$\gamma_H = \frac{E_H}{RT_o}, \quad \gamma_L = \frac{E_L}{RT_o},$$

$$\mu_H = \frac{\tilde{\mu}\rho^0_{fH}}{\rho_{gi}Y_i}, \quad \mu_L = \frac{\tilde{\mu}\rho^0_{fL}}{\rho_{gi}Y_iY_H},$$

$$\mu_{gH} = \frac{\tilde{\mu}\rho^0_{fH}}{\rho_{gi}}, \quad \mu_{gL} = \frac{\tilde{\mu}\rho^0_{fL}}{\rho_{gi}},$$

$$q_H = \frac{Q_H\rho^o_{fH}}{(1-\phi)c_s\rho_sT_o}, \quad q_L = \frac{Q_L\rho^o_{fL}}{(1-\phi)c_s\rho_sT_o},$$

$$\dot{A}_H = \frac{a_s\alpha_skpY_i}{q_HE_Hl_\eta v_i^2}, \quad \dot{A}_L = \frac{a_s\alpha_skpY_HY_i}{q_LE_Ll_\eta v_i^2},$$

$$Y_H = \frac{1-\mu_HV_{DH}}{1+\mu_{gH}V_{DH}} \quad \text{and} \quad Y_L = \frac{1-\mu_LV_{DL}}{1+\mu_{gL}V_{DL}}.$$

Note that the information related to the stoichiometry and kinetics of each reaction is included within these parameters.

As in the previous case with the single-reaction region, Table 3.1 includes the base-state values for the HTO parameters. In the following section, the system of equations are solved to estimate the temperature profile across the coupled reaction regions and to analyze the effect of varying fuel mass densities (in terms of $R_F=\rho^o_{fL}/\rho^o_{fH}$) reaction heats (in terms of $R_Q=Q_L/Q_H$), activation energies (in terms of $R_E=E_L/E_H$), injection rate and external heat losses (in terms of reservoir thickness) on propagation of reaction regions. The analysis will obviously be based on the temperatures of the reaction regions, their common steady-state propagation speed and their distance of separation.

While performing these calculations, it is desired that the results could be directly comparable to the single-reaction front propagation of the previous section. In order to achieve this, it is required that the two-reaction combustion front propagation is thermally calibrated. This could be done by simply keeping the total heat content of the reservoir always the same: i.e., $q_H + q_L = q$. As shown in the Appendix A, this condition can be equally represented in terms of the following expression:

$$R_F = \frac{1}{R_Q}\left(\frac{1}{\alpha} - 1\right) \tag{12}$$

$\alpha = \rho^0_{fH}/\rho^0_f$ is defined as the ratio of the fuel generated for the HTO front and the fuel *a priori* available for the single reaction combustion front. Also note that, the equation (12) is also dependent on the ratio of the heat of reactions R_Q. The latter, however, will be kept constant during the work. When $Q=Q_H$ (as given in Table 3.1), and $R_Q = 1/2$ is taken, then, for example, for $\alpha = 1/2$, $R_F = 2.0$ should be kept in the calculation. Hence, during the analysis, while parameter α is varying between (1,0), R_F should change according to (12) in the range of $(0,\infty)$.

CHAPTER 4

DISCUSSION AND RESULTS

4.1 Adiabatic Reaction Regions

In the adiabatic case, h =0 is taken in equation (6). It is important to note that in this case the HTO front temperature will not be affected to any substantial degree from whether or not the conditions of coherence exist. Indeed, the analysis of Akkutlu and Yortsos (2004) shows directly that its dimensionless temperature would be

$$\theta_{fH} \equiv \frac{T_{fH}}{T_o} \cong 1 + q_L + q_H \tag{13}$$

However, the coherence does affect the LTO front temperature:

$$\theta_{fL} = 1 + q_L + q_H \exp\left(-V_{DL}\xi^*\right). \tag{14}$$

Hence, under the adiabatic condition, only the latter is influenced (coupled) by the common front propagation speed V_D. Figure 4.1 shows estimated properties of the coherent reaction regions versus air injection velocity for varying R_E. (Here, the ratio is varied by fixing E_H to its value as given in Table 3.1 and varying E_L only.) The LTO front temperature in Figure 4.1a changes with the injection velocity and takes values as low as 250°C depending on the contrast between the activation energies of the two-reaction combustion system. The estimated front velocities are the same order of magnitude in relative to single-reaction case (Figure 3.1), yet they are not influenced by R_E and do not change significantly with the air injection rate (Figure 4.1b). This behavior is an indication of reactive system being kinetically controlled, i.e., temperature-

dependent. It is also observed in Figure 4.1 that the common propagation speed of the reaction regions is overwhelmingly controlled with the constant temperature of the HTO front, since changes in neither the LTO front temperature (Figure 4.1a) nor the separation distance (Figure 4.1c) appear to be influential. Further, there exists a range of air injection velocities for the coherent front propagation. This velocity range is the largest for R_E values greater than 0.7; it is smaller for intermediate values; it shrinks and becomes negligibly small for values equal to or less than 0.6. In further detail, for R_E =0.4, the coupled steady-state front propagation is observed only for injection velocities in between 297.4- 298.0 m/day, which is such a small range that could be safely considered as constant; thus, its corresponding curve appears as a vertical straight line on Figure 4.1c. At lower velocities, no solution exists for the adiabatic reactive system.

Behavior of the reaction regions at low R_E requires further attention. For R_E =0.7 curve in Figure 4.1c, it can be seen clearly that the distance between regions increases with the injection velocity. At the intermediate values, the relationship is linear and the reaction regions accelerate with the air injection velocity. As the velocity approaches to point *B* however, the distance-velocity relationship becomes strongly nonlinear. In the vicinity of this critical point, the distance between the fronts appears to change asymptotically with the injection velocity, thus, a small velocity change in this region could lead the fronts to be infinitely-separated and, hence, thermally de-coupled. Physically this local nonlinear behavior should correspond to conditions where the self-sustaining reaction regions could no longer cohere in the reservoir. Beyond this limit, i.e., at injection velocities larger than the value at point *B*, no real solutions are obtained; therefore, de-coupled, i.e., fully separated, propagation is expected. Similarly, when the curve corresponding to R_E =0.4 is considered instead, the reaction regions have difficulty to propagate coherently in the reservoir and tend to become easily de-coupled regardless of the injection velocity.

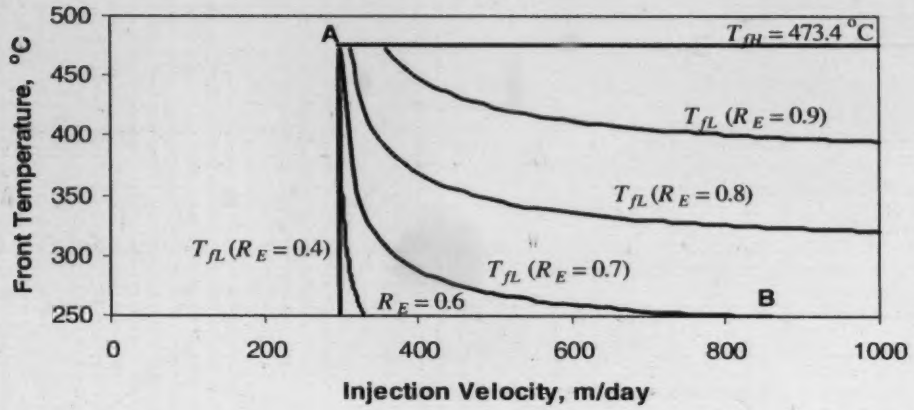

(a)

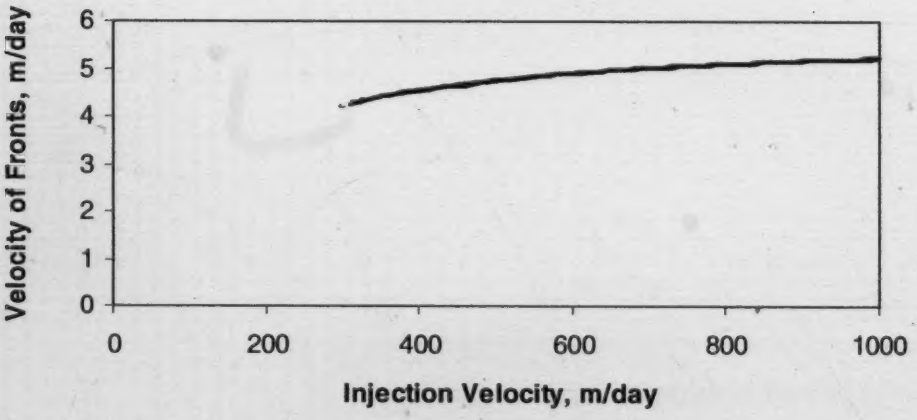

(b)

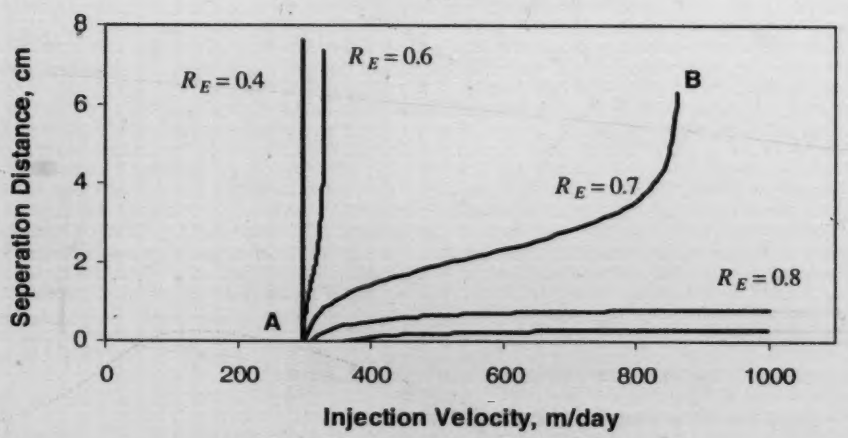

(c)

Figure 4.1 - Properties of the adiabatic coherent front propagation versus injection velocity for varying activation energy ratio, R_E. R_Q=0.5, α=0.6, R_F=1.33.

The nonlinear behavior at the other end of R_E =0.7 curve near point *A* on Figure 4.1c, however, should not be treated similarly. At this end, the reaction regions are located close to each other; therefore, the regions have difficulty to keep their sequential and self-sustaining nature under this low-injection limit.

Adiabatic model predicts that the reaction regions could self-sustain and propagate in the reservoir within a distance from each other. Two limits are found: the fronts could coincide (with a distance nil) in the lower limit at point *A*; and they could become infinitely-separated and de-coupled beyond point *B*. The extent of these limits in the injection velocity space varies significantly with the activation energies of the reactions.

The effect of R_F on the adiabatic system is also investigated. As it was mentioned earlier, changing R_F in our models points to a change in the stoichiometric coefficient of the fuel-generating LTO reaction. Thus, the larger R_F value is, the greater the fuel generation efficiency of the combustion system becomes. For the activation energy ratio equals to 0.7, the values for injection velocities, which are uniformly distributed between points A and *B* (Figure 4c), are selected: 400, 600 and 800 m/day. The estimated properties of the coherent reaction regions are shown in Figure 4.2 for these injection rates. (Dashed lines on these figures show that there is no solution). From the figure it can be seen that, in the limit $R_F \rightarrow 0$, the estimated combustion front velocity is 3-4 m/day (Figure 4.2b), although the LTO front is located far ahead of the HTO (Figure 4.2c) and its front temperature approaches to the initial reservoir temperature (Figure 4.2a). In essence, in this limit, the two-reaction combustion front yields solutions identical with the single-reaction case, i.e., the case with a reservoir containing *ab initio* fuel.

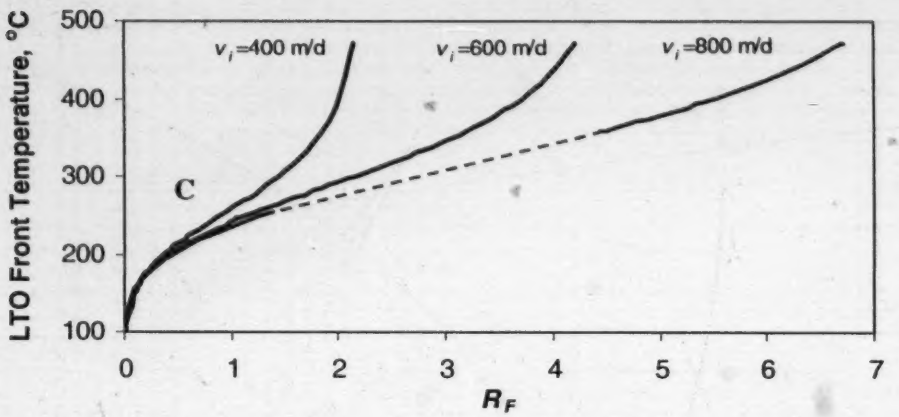

(a)

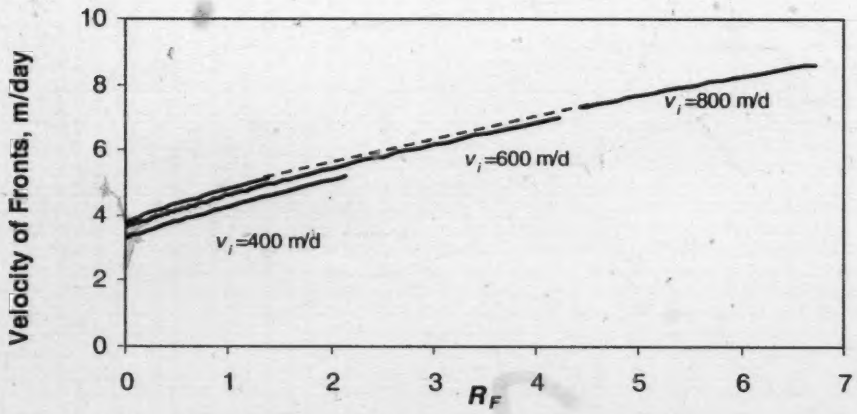

(b)

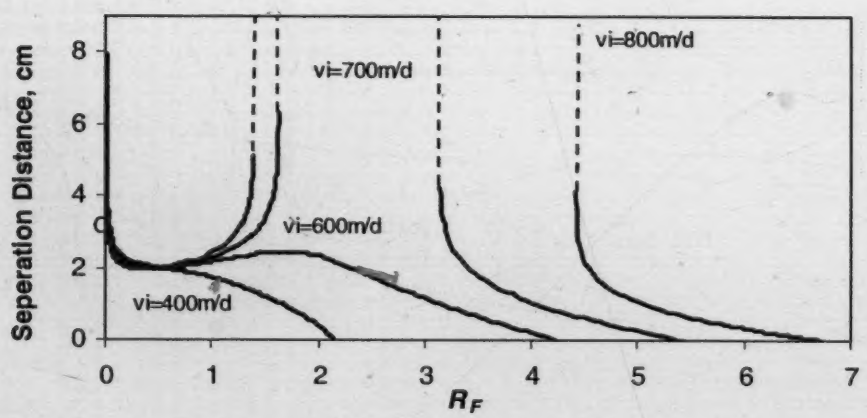

(c)

Figure 4.2 - Properties of the adiabatic coherent front propagation versus fuel ratio R_F for varying injection velocities. R_Q=0.5, R_E=0.7.

As R_F of the system is increased and approaches to point C, the fronts drift towards each other and settle within a separation distance of about 2cm; meanwhile, the LTO front temperature becomes higher than 200°C. Hence, Figure 4.2 suggests that, in order to understand the behavior of the two-reaction system with high levels of fuel generation efficiencies, one should make a rigorous analysis of the trends in the sections of the parameter space, where R_F becomes larger than the value at Point C.

At intermediate R_F values, on the r.h.s. of point C in Figures 4.2a and 4.2c, the system follows two different paths depending on the magnitude of injection velocity: (1) at moderate velocities, e.g., v_i=400-600 m/day, coherent propagation occurs with increasing R_F as the fronts further approach each other; (2) at high velocities, the propagation could take place at higher values of R_F yet without the necessity of fronts approaching each other. In the former case, the overall trend in terms of front separation distance is much like the oil/water capillary pressure characteristics during a spontaneous imbibition process (where S_W plays the role of R_F); whereas, in the latter case, it could appear as an asymmetric U-shaped curve. Thus, the interaction of the fronts is strongly nonlinear and, depending on the injection rate and LTO stoichiometry, the fronts could be completely separated from each other once again. At large R_F values, however, the fronts appear to approach each other once again. In the latter case the separation distance becomes smaller exponentially with the increasing R_F values. The rate of decrease is controlled by the injection, distance diminishing with a larger rate as the injection is increased. These trends are shown in Figure 4.2c and suggest the following explanation. Once equation (14) is re-arranged for the nondimensional separation distance ξ^*, the following expression is obtained:

$$\xi^* = \frac{-1}{V_D} \ln\left[\frac{(\theta_{fL} - 1) - q_L}{q_H}\right]. \tag{15}$$

Accordingly, positive and real distances are observed when the following condition is satisfied:

$$0 < \frac{\theta_{fL} - 1}{q_H} - R_Q R_F < 1.0 \qquad (16)$$

Hence, the distance should increase as the argument of the inequality approaches to zero, and decrease as it advances towards unity. In the limit $R_F \rightarrow 0$, the second term of the argument ($R_Q R_F$) approaches to zero. However, the first term also approaches to zero (since $\theta_{fL} \rightarrow 1$) and at a larger rate; thus, significantly large distances are observed in this limit. As R_f increases the first term increases either with a larger rate, hence, the argument of inequality grows, approaching to unity (this trend is observed with the v_i=400 m/day curve on Figure 4.2c); or with a rate not necessarily larger than the constant rate of R_F change. In the latter case, the argument approaches to zero and the fronts become separated once again, but, this time, for an LTO front with high fuel generation efficiencies. The latter effect appears beyond point C at the intermediate R_F values and becomes more pronounced at large injection velocities, hence generating the asymmetric U-shaped curves. The argument could become even less than zero at these large velocities; At higher R_F values, the condition of inequality (16) is satisfied once again and the argument increases towards 1 as the distance of fronts becomes exponentially smaller.

The results of adiabatic reaction regions suggest that the behavior of the two-reaction combustion system is essentially controlled by the chemistry of in-situ fuel generation. During the analysis, however, the external heat losses were neglected. In return, the HTO front temperature was fixed to a constant value; hence, the size of the problem was reduced significantly. In the following h =0 condition is relaxed and investigation is extended to understand the behavior of thermodynamically open reactive system with sequential reaction regions.

4.2. Non-adiabatic Reaction Regions

When the two reaction regions are coupled and travel coherently under the influence of convective heat transfer to the surroundings the front temperatures are given by Akkutlu and Yortsos (2004) as

$$\theta_{fH} = 1 + \frac{q_H}{\Delta_h} + \frac{q_L}{\Delta_h} \exp\left[-\frac{1}{2}(\Delta_h - 1) V_{DH} \xi^* \right] \tag{17}$$

and

$$\theta_{fL} = 1 + \frac{q_L}{\Delta_h} + \frac{q_H}{\Delta_h} \exp\left[-\frac{1}{2}(\Delta_h + 1) V_{DL} \xi^* \right], \tag{18}$$

where Δ_h and h are as given before during the description of equation (2). Sensitivity analysis, in this case, addresses the combined effects of the external heat losses with the injection velocity and with R_F. For this purpose, the coupled algebraic equations (10), (11), (17) and (18) are simultaneously solved; the non-adiabatic system behavior is compared with the solutions of equation (6) in three regions. The results consistent, showing that both approaches yield the same behavior in the presence of reservoir heat losses.

Figure 4.3 shows temperature profiles for the non-adiabatic sequential reaction case for fuel densities of ρ^o_{fL}=21.0 kg/m^3 (Figure 4.3a) and ρ^o_{fL}=25.0 kg/m^3 (Figure 4.3b). It can be seen that the temperature profile and separation distance are quite sensitive to the variation in the fuel density. As the LTO fuel density increases, a slight decrease in the HTO front temperature and a non-monotonic variation of the LTO front temperature are observed. The front velocity decreased weakly and separation distance increased (Akkutlu and Yortsos, 2004).

The combined effects of the external heat losses with R_F are shown in Figure 4.4. It is noticed that the range of R_F where coherence is observed is enlarged. Figure 4.4a shows that the non-adiabatic LTO front temperature is lower. While R_F increases, the HTO (LTO) front temperature decreases (increases) until they eventually have the same temperature values, see the intersection points I_1, I_2 and I_3 in Figure 4.4a.

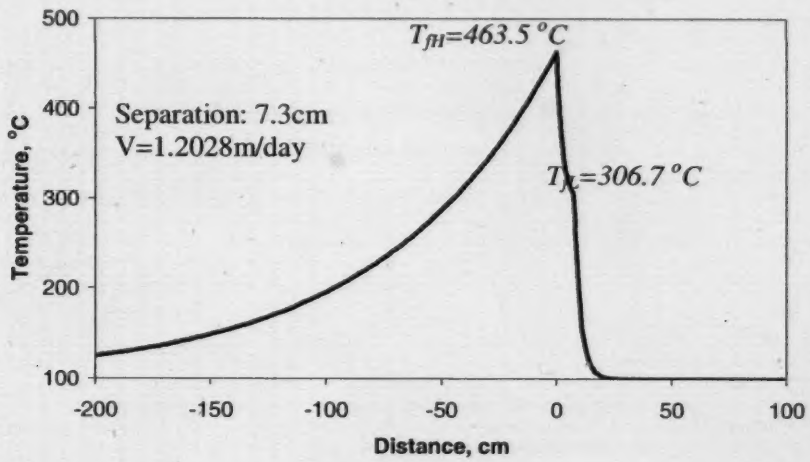

(a)

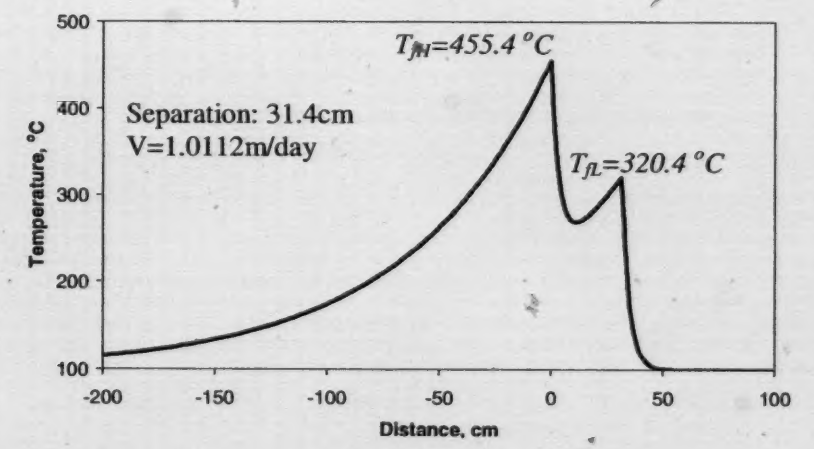

(b)

Figure 4.3 - Non-adiabatic temperature profiles of the sequential reaction regions for varying amount of hydrocarbon deposition. (a) ρ^o_{fL}=21.0 kg/m^3, (Y_H=0.6246, Y_L=0.0021). (b) ρ^o_{fL} =25.0kg/m^3 (Y_H=0.6242, Y_L=0.0014)

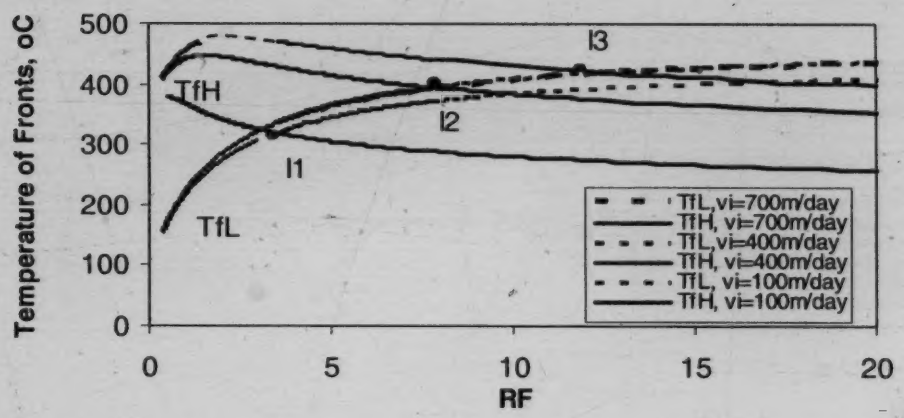

(a)

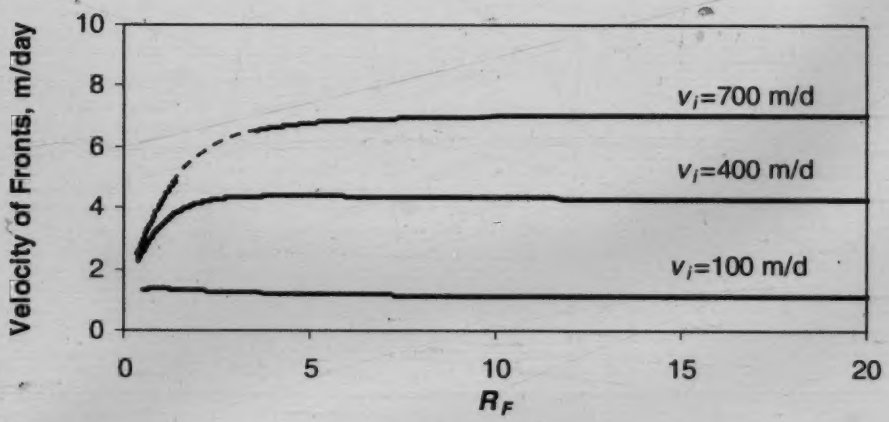

(b)

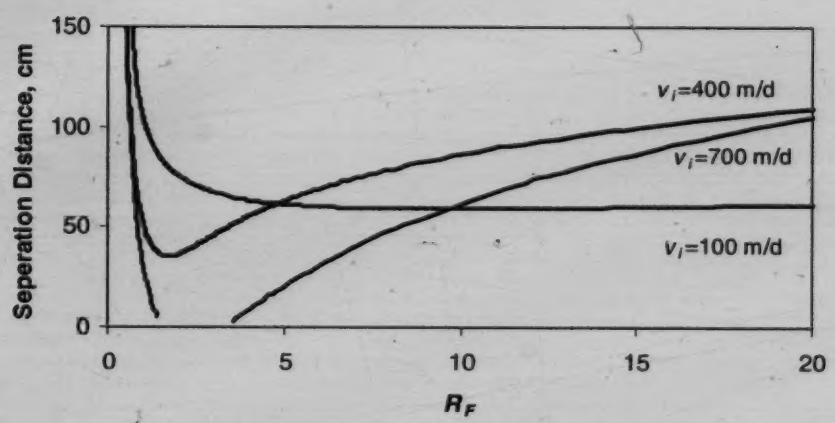

(c)

Figure 4.4 - Properties of the non-adiabatic coherent front propagation fuel ratio R_F for varying injection velocities. R_Q=0.5, R_E=0.7. Constant heat loss rate: $\tilde{h}/H$=0.039 kW/m^3-K.

Note that the temperatures of the fronts become identical with a finite separation distance, see Figure 4.4c. Interestingly, the estimated distances are nearly the same and roughly around 60-70 cm for all the considered injection velocities. At higher R_F values, the HTO front temperature continues to drop and becomes less than the LTO front temperature. At lower injection values, the contrast between the temperatures of reaction regions is drastic, see the front temperature curves on Figure 4.4a corresponding to v_i=100 m/day. Meanwhile, at high R_F values, the estimated common propagation speed is nearly constant and independent of R_F.

In the presence of heat losses, the reaction regions have the ability to propagate coherently with a larger distance from each other. It appears to be normal for these fronts to keep a distance in O (10 cm), see Figure 4.4c. This strictly was not the case when the system was thermally insulated when the fronts tended to either propagate much closer to each other (with a distance in the order of 1 cm) or become fully separated.

Figure 4.5 permits to quantitatively compare solutions with the adiabatic results. Figure 4.5a shows that, much like in the case of single-reaction combustion fronts, the temperatures of the reaction regions merge with the adiabatic solutions at high air injection velocities. Whereas the external heat losses start dominating the system as air injection velocity is decreased. The influence is drastic on HTO front temperature (Figure 4.5a) and common speed of coherent propagation (Figure 4.5b), values dropping below 300°C and 1 m/day respectively. One should also note the difference with the adiabatic propagation speed. The latter is almost leveled off and has reached the kinetically-controlled front propagation limit; whereas, in the presence of external heat losses and at low injection velocities, the system becomes stoichiometrically controlled, hence, the common propagation speed becomes directly proportional to the air injection rate.

Among the trends in Figure 4.5, perhaps the most interesting and even puzzling one is the effect of heat losses on the separation distances of the fronts. Most importantly, in the presence of heat losses, the asymptotic behavior near the critical point B (of Figure 4.5c) disappeared. Furthermore, now distances are estimated inversely proportional to the same

injection velocities in between points *A* and *B*. This inverse behavior persists at large heat loss rates. Secondly, in the presence of heat losses, the lower limit near the critical point *A* practically does not exist anymore; now, the fronts could self-sustain and propagate (with a low speed though) at injection velocities as low as *O* (10 m/day). In essence, it is observed that a small intensity of heat loss rate to the surroundings actually could increase the range of injection velocity for coherent propagation of the reaction regions and support the combustion front propagation at low injection rates.

Another advantageous effect of the external heat losses on the two-reaction combustion system can be easily identified once the effect of heat loss intensity is investigated. As shown in Figures 4.5 and 4.6 intensity can be changed under reservoir conditions by means of varying the convective heat transfer rate coefficient $\tilde{h}/H$. Previously it is observed in Figure 3.2 that the single-reaction front temperature drops and the front slows down with the increasing heat loss rates. Interestingly, in the case of two-reaction system, these properties are not significantly affected with the variations in heat loss rate; the influence of heat losses is almost negligible. These are clearly shown in Figure 4.5a and 4.5b. On the other hand, the heat loss rate affects significantly the distance between the fronts (Figure 4.5c and 4.6), with the fronts getting closer to each other as the intensity of heat transfer to the surroundings is increased. In the mathematical framework, this could be interpreted as the left-hand-sides of equations (10-11), and (17-18) staying nearly constant regardless of the magnitude of the imposed Δ_H value with the only expenditure of decreasing ξ^*. Essentially, the fronts tend to minimize the effects of external heat losses and increase their ability to self-sustain, simply by approaching to each other. Consequently, extinction of the fronts is prevented even though under the same conditions extinction has developed in the form of multiplicity for the single-reaction combustion front (Figure 3.2). Sustained propagation of the two-reaction combustion fronts is not warranted, however, since at lower injection velocities the single-reaction front temperature will continue to decrease rapidly.

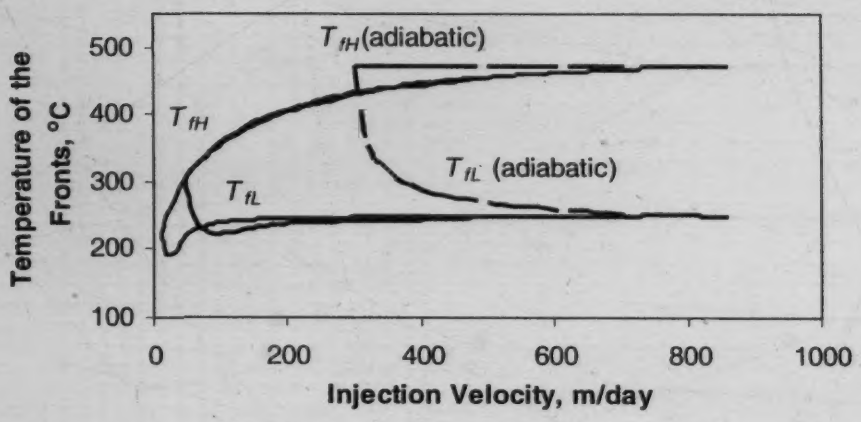

(a)

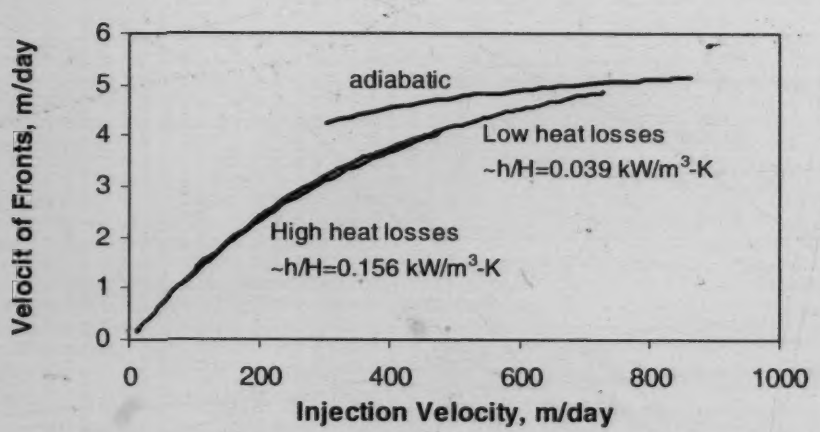

(b)

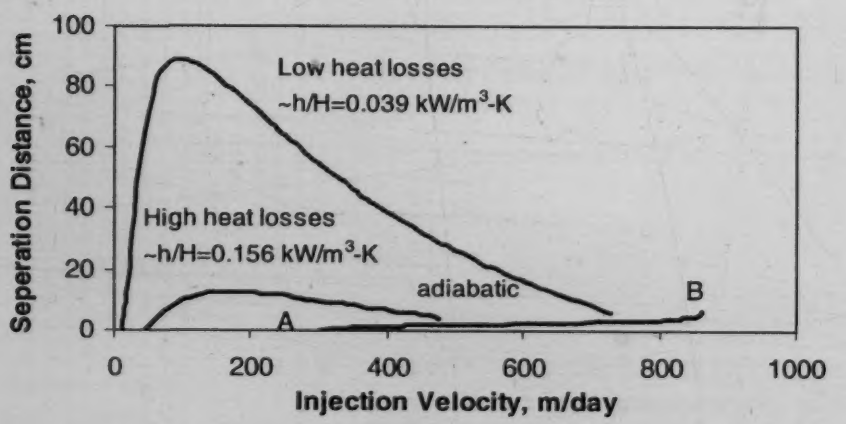

(c)

Figure 4.5 - Properties of the non-adiabatic coherent front propagation versus injection velocity. R_Q=0.5, R_E=0.7, α=0.6, R_F=1.33.

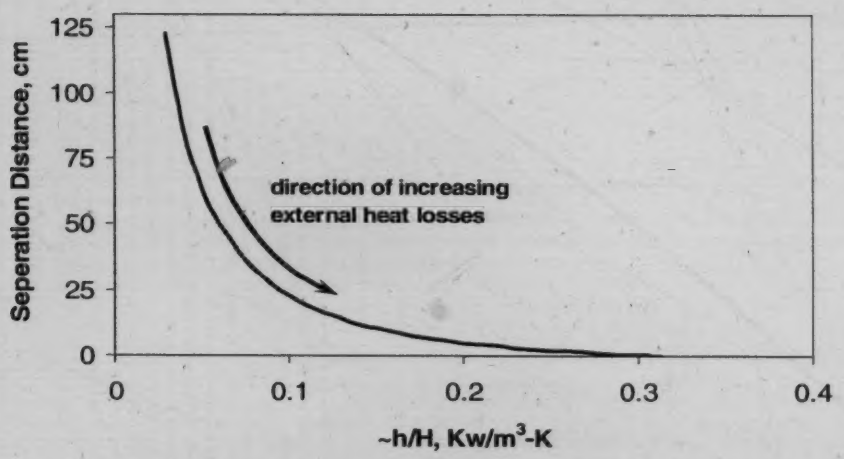

Figure 4.6 - Separation distance of the non-adiabatic fronts versus the external heat loss rate coefficient. R_Q=0.5, R_E=0.7, α=0.6, R_F=1.33.

4.3 Combustion Front Propagation in the Presence of Catalytic Agents

4.3.1 Catalytic Effect

The presence of catalytic agents influences combustion front propagation through the quantities γ and A of equations (10) and (11) due to their dependence on the frequency factor, k, specific fuel surface area, a_s, and activation energy, E.

4.3.1.1 Activation Energies

An increase in the value of activation energy means that chemical transformation has to overcome higher energy barrier related to the energy of the covalent bonds. The required amount of reaction energy is provided by the kinetic energy of translational motion of the colliding oxygen and hydrocarbon molecules, i.e, two-body collisions. If initially heat is released and local temperature becomes larger, the mean kinetic energy of the molecules will soon increase, and thus a greater number of colliding molecules will have sufficient amount of kinetic energy to overcome the energy barrier. Thus, in accordance with the

Arrhenius dependency, the reaction rate increases. If the reaction is accelerated, more heat will be released, the temperature of the medium will further increase, and the reaction will be further accelerated. Therefore, an increase in activation energy of a reaction leads a steadily propagating reaction region to higher temperatures.

This explanation is strictly valid for the energy and temperature relationship of an HTO reaction region in the presence of a preceding LTO region. Table 4.1 shows all the possible changes in activation energies at a constant velocity and corresponding change in HTO front temperature calculated by the model. Four cases are observed where the HTO temperature increases: cases 2, 4, 6 and 8. Only Case 8 among them has the potential to increase the temperature significantly. This is also the case during the kinetics experiments of He *et al.* (2005), when water soluble Fe^{+} is added to a silica-Cymric heavy oil and to a kaolinite-Cymric light oil mixtures.

Figure 4.7 shows the effect of variations in the activation energies on the reaction region dynamics, in accordance with Case 8. It is clear that a contrast in activation energies improve the HTO temperature significantly at high air injection rates. Although, the

Table 4.1 - Influence of 5% Change in Activation Energies on HTO Temperature (v_i=100m/day)

Case	E_H	E_L	HTO temperature, °C
1	↓	base	↓ 22.33 °C
2	base	↓	**↑ 4.45 °C**
3	↓	↓	↓ 19.81 °C
4	↑	base	**↑ 19.42 °C**
5	base	↑	↓ 7.66 °C
6	↑	↑	**↑ 6.38 °C**
7	↓	↑	↓ 26.71 °C
8	↑	↓	**↑ 27.13 °C**

catalytic effect becomes smaller as the injection is decreased due to the presence of reservoir heat losses.

It is clearly indicated in Figure 4.7 that, at higher injection rates, the reaction regions approach each other, Figure 4.7c, and eventually overlap at around 300 m/day. Thus, there exist no solutions corresponding to coherent propagation at higher injection rates.

The changes in activation energies have negligible influence on the estimated LTO temperatures, which is nearly a constant for a large range of air injection rate.

Results indicate that the observed improvement in self-sustainability of the combustion process could perhaps be attributed to a catalytic effect originating from a contrast in the HTO and LTO activation energies. Combustion tube runs of He *et al.* (2005) also support this observation. Interestingly, however, their kinetics experiments corresponding to Case 8 predicted 30-40°C lower HTO temperatures than the base values. The latter then appears to be in contradiction with the observed improvement. Here, it is shown that the estimated HTO temperature indeed increases and the estimates using the kinetics experiments, however, may not reflect this improvement, since the latter are based on zero-dimensional observations and, therefore, do not exhibit any interaction between reaction regions during their propagation.

4.3.1.2 Frequency Factors

An increase in value of reaction frequency factor causes the reaction rate to proportionally increase, which, consequently, is expected to accelerate the reaction region propagation and its temperature. Similarly, considering cases 1-8, the influence frequency factors on the HTO temperature is investigated with a 5% change in their values. Table 4.2 shows that the reaction temperatures do not necessarily obey the expected variations. This points out to a complex interplay of the reaction regions during the in-situ combustion process. Clearly the HTO temperature variations are much smaller than those due to variations in the activation energies.

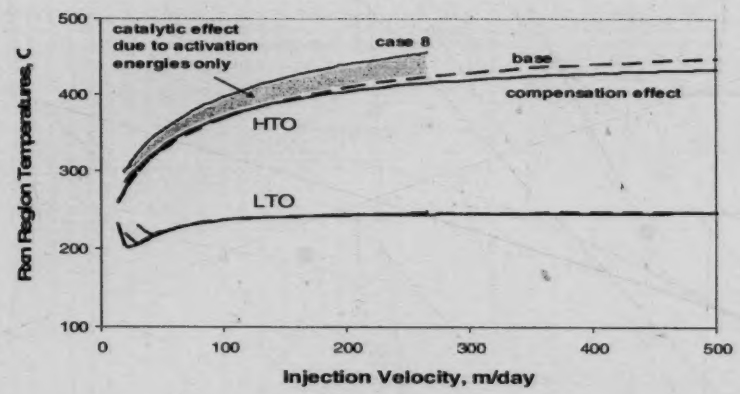

(a)

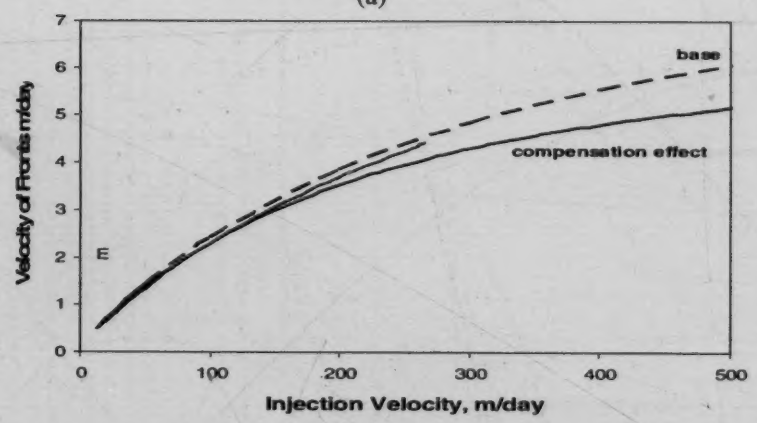

(b)

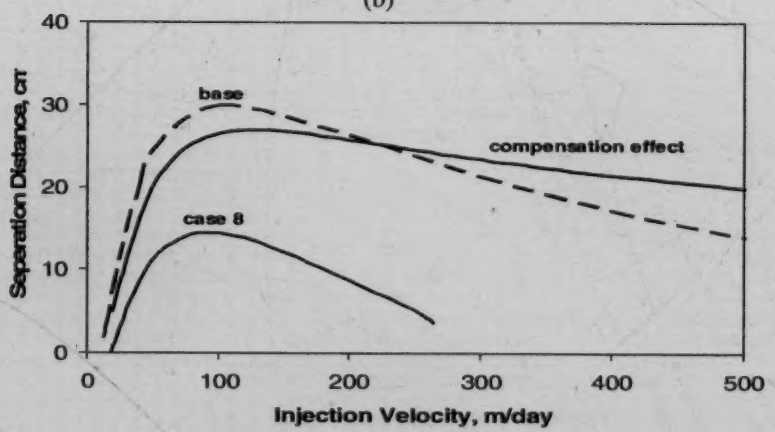

(c)

Figure 4.7 - Catalytic Effects on In-situ Combustion Process. Reaction region (a) temperatures, (b) propagation velocity and (c) separation distance versus air injection velocity.

Table 4.2 - Influence of 5% Change in Frequency Factors on HTO Temperature (v_i=100m/day)

Case	k_H	k_L	HTO temperature, °C
1	↓	base	↑ 1.88 °C
2	base	↓	↓ **0.45 °C**
3	↓	↓	↑ 1.42 °C
4	↑	base	↓ **1.77 °C**
5	base	↑	↑ 0.42 °C
6	↑	↑	↓ **1.36 °C**
7	↓	↑	↑ 2.30 °C
8	↑	↓	↓ **2.23 °C**

4.3.1.3 Specific Fuel Surface Areas

Based on the formulation of the model, i.e., equations (10) and (11), the influence of hydrocarbon fuel surface areas should be identical with the frequency factors. Hence, HTO temperature changes observed in Table 4.2 is equally valid for the fuel surface areas.

4.3.1.4 Combined Effects of the Activation Energies and Frequency Factors

The estimated temperatures in Tables 4.1 and 4.2 are such that, in all the cases considered, the temperature change due to the activation energies consistently offsets the change due to frequency factors. Thus, it becomes an important issue for the analysis whether the activation energies and frequency factors of the reactions vary independent of each other in the presence of catalytic agents, or not.

Often, a change in activation energy has been considered as an indication of the catalytic activity. However, Drici and Vossoughi (1985) showed that consideration of the changes in the energy alone can be misleading; instead, combined (compensation) effect of the frequency factor and activation energy of a reaction should be considered throughout an investigation. Here, a normal (m>0) compensation effect is considered for the HTO and LTO reactions i.e, the frequency factor and activation energy relationship of the oxidation reactions follows a positive trend, in the presence of catalytic agents:

$$\log k = mE + c \tag{19}$$

where m=6.453E-5 kmole/kJ is given by Drici and Vossoughi (1985) and valid in the presence of various metal oxides and c = -2.38 is taken here so that the base-state values of activation energies and frequency factors are recovered using equation (19). Figure 4.7 also shows the compensation corresponding to Case 8 in terms of the changes in temperatures, propagation velocities and separation distances of the reaction regions. It clearly shows that the compensation effect indeed eliminates the previously observed catalytic effect due to contrast in the activation energies only. The estimated HTO temperatures and velocities are nearly identical to the base-state solution at low and moderate air injection rates; at high rates, the estimates become even less than the predicted base values.

The results distinctly illustrate that the changes in kinetics due to catalytic agents in porous media has the potential to influence, in particular, properties of the HTO region. This catalytic effect, however, could be eliminated in the presence of a normal compensation effect.

Table 4.3 -Influence of 5% Change in Hydrocarbon Fuel Densities on HTO Temperature (v_i=300m/day)

Case	ρ^o_{fH}	ρ^o_{fL}	HTO temperature, °C
9	base	↑	↑ 1.64 °C
10	↑	↑	↑ 3.52 °C

4.3.2 Fuel Deposition Effect

Presence of clays, metallic minerals and additives may change the specific surface are of the porous medium, consequently, vary hydrocarbon fuel deposition and, hence the total heat content of the reservoir. Therefore, dynamics of the coherent reaction regions is expected to be influenced by the dimensionless quantities q in equations (17) and (18), A (due to dependency on q) and Y (due to dependencies on μ and μ_g) in equations (10) and (11).

Sensitivity of the HTO temperature on the fuel densities are given in Table 4.3. The cases consider the possibility of increased hydrocarbon deposition ahead of the LTO reaction region. Notice that, with respect to temperature variations due to activation energies given in Table 4.1, the HTO temperature increases only slightly even though the air injection rate is three times larger. Regardless, Table 4.3 also shows that the temperature increase of Case 10 is about two times large than that of Case 9. Figure 4.7 shows the combustion behavior with Case 9 when the hydrocarbon deposition ahead of the LTO is doubled. Estimated values of the HTO temperature are much lower than the base values at air injection velocities below 400 m/day; at higher injection rates, however, there exists a small region of increased combustion performance due to increased hydrocarbon deposition. At higher (lower) air injection (heat loss) rates, it is expected that the region of improved combustion performance is much larger.

Figure 4.8 also shows that, unlike the catalytic effect of §3.1, the hydrocarbon deposition causes dramatic changes in the LTO temperature. At low and moderate air injection rates (35-200 m/day) its estimated values increase such that the LTO temperature becomes even larger than the HTO temperature. Hence, in this region, control over the combustion performance shifts from HTO and is dictated by the LTO region. This observation is in agreement with the experimental results of Drici and Vossoughi (1985), where, using thermal analysis techniques, the authors predicted a shift of a large amount of heat from a high to a low temperature range due to an increase in the solid surface area in the presence of clays. Nevertheless, the results show that the overall influence of this shift may not be strong enough to improve the combustion performance.

Figure 4.9 shows combustion behavior due to fuel deposition in accordance with Case 10. In this case, the hydrocarbon amount ahead of the LTO region is 50% larger than the base value and the HTO fuel amount increases proportionally. Thus, the total heat content of the reservoir is the same as in Case 9, i.e., two times larger than the base-state, hence, Figures 4.7 and 4.8 are comparable.

At high air injection rates, it is clear that the increased fuel amounts significantly affect both reaction region temperatures, which consequently, improves the combustion performance. As the injection rate decrease, however, separation distance of the reaction regions increase, which promotes the heat transfer to the surroundings and, consequently, the enhancement on the combustion performance disappears. Estimated variations in the separation distance are shown in Figure 4.10. Note that the predicted distances with case 10 are significantly larger than Case 9 and the base-state. As the air injection rate is decreased, the distance increases nonlinearly and, at the rate v_f=230 m/day, it becomes infinitely large, namely the reaction regions are fully-separated. At low injection rates, there exist solutions correspond to the coherent propagation of reaction regions with a finite distance; however, the predicted temperatures are close to the base-state values. The estimated coherent propagation velocity of the reaction regions with cases 9 and 10 does not show significant variations from the base values.

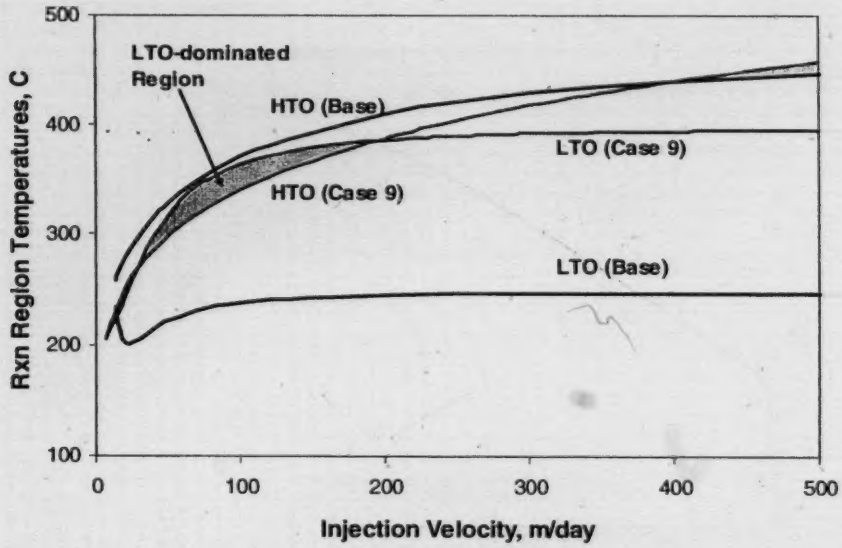

Figure 4.8 - Hydrocarbon Deposition Effect on In-situ Combustion (Case 9): Temperatures of the reaction regions versus air injection velocity. The hydrocarbon amount ahead of the LTO region is two times larger than the base value.

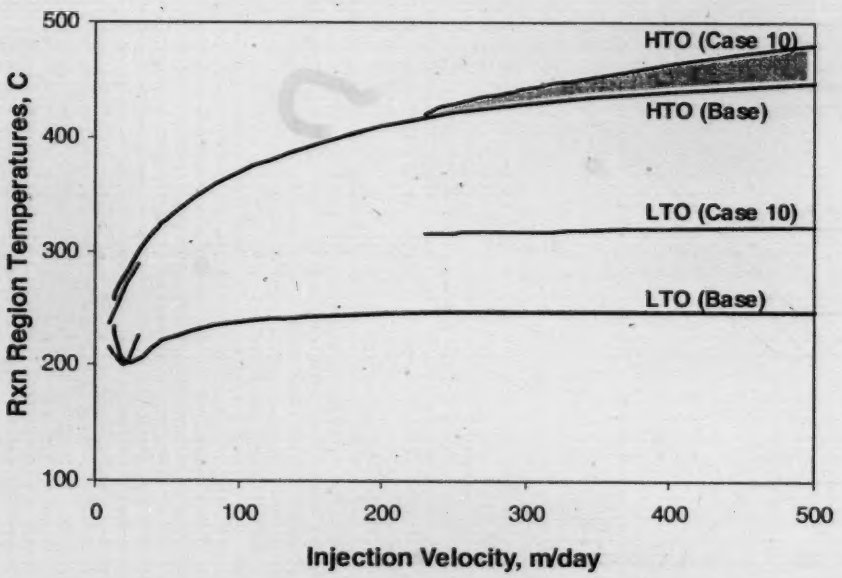

Figure 4.9 -Hydrocarbon Deposition Effect on In-situ Combustion (Case 10): Temperatures of the reaction regions versus air injection velocity. The hydrocarbon amount ahead of the LTO region is 50% larger than the base value.

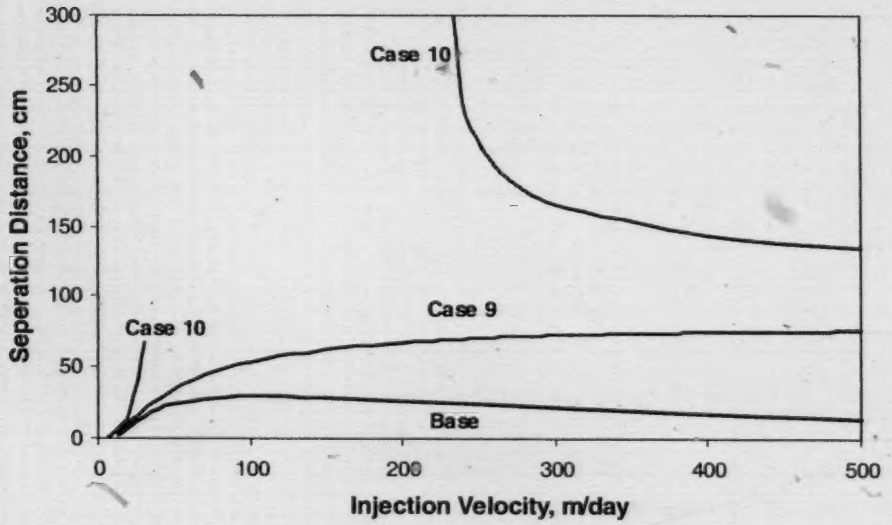

Figure 4.10 - Hydrocarbon Deposition Effect on In-situ Combustion (Cases 9 and 10): Separation distance of HTO and LTO reaction regions versus air injection velocity.

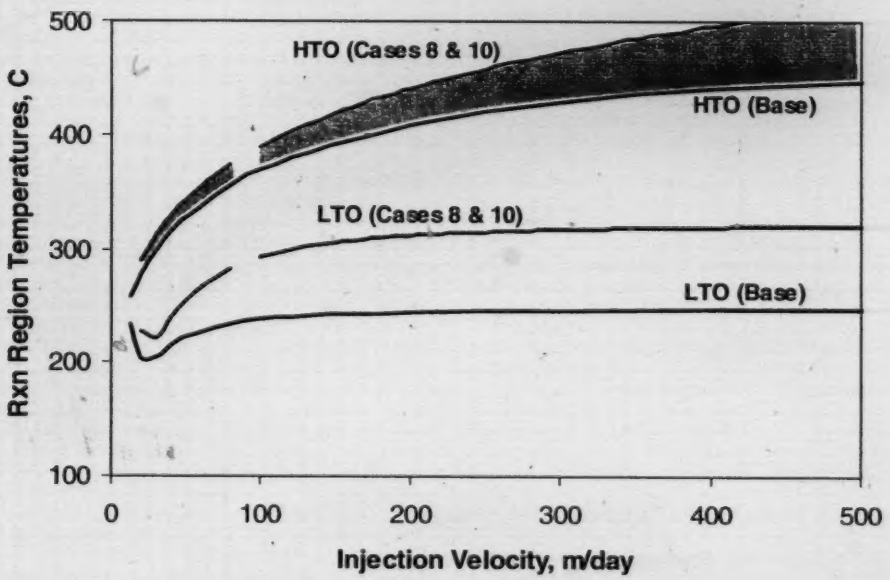

Figure 4.11 a- Dual Effect (Case 8 + Case 10) of Clays/Additives on front temperatures

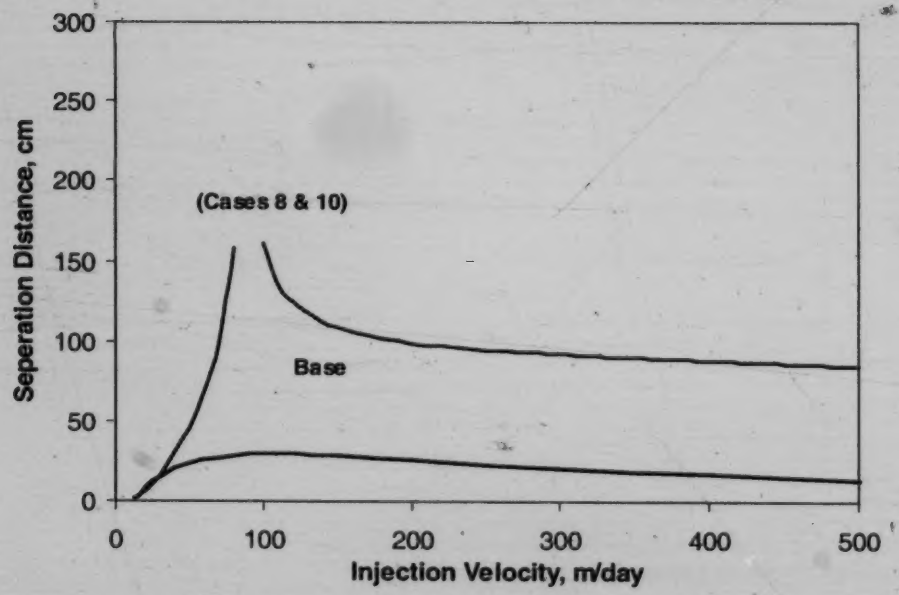

Figure 4.11 b- Dual Effect (Case 8 + Case 10) of Clays/Additives on separation distance

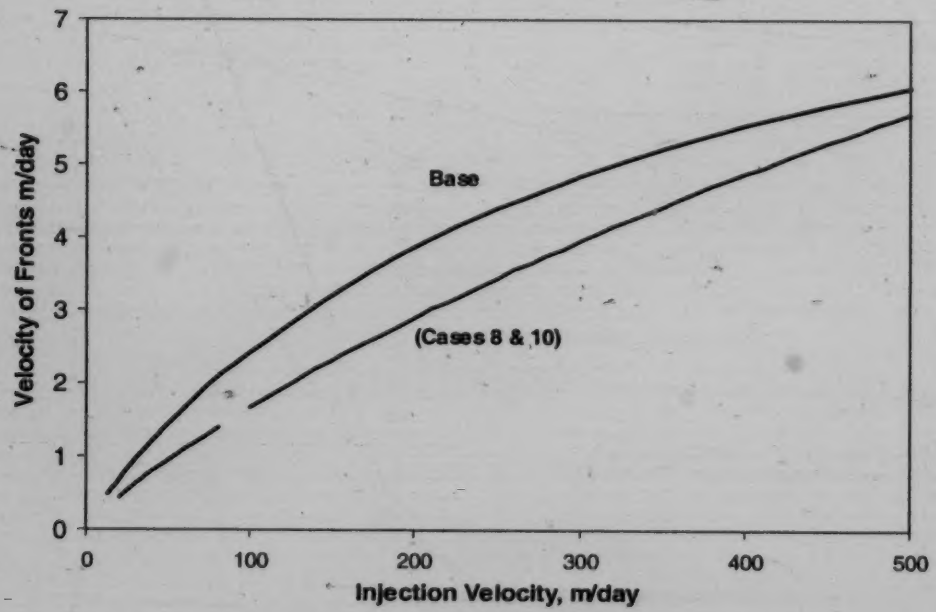

Figure 4.11 c- Dual Effect (Case 8 + Case 10) of Clays/Additives on propagation velocity

In essence, the results of this section point out the importance of HTO fuel generation stoichiometry on the combustion behavior. Case 10 considered generation of an additional amount of fuel for the HTO region, although the total amount of hydrocarbons is the same as in Case 9.

4.3.3 Combined (Dual) Effects

In this section combined catalytic (Cases 8) and hydrocarbon deposition (Case 10) effects of catalytic agents without compensation are considered. The results could be equally considered as the catalytic effect with compensation where the changes in reaction rates are due to specific surface area of the HTO and LTO hydrocarbon fuels.

Figure 4.11 shows that dual effects of the materials noticeably improve the combustion performance in the presence of reservoir heat losses. The HTO temperature reaches to values larger than 500°C and the LTO temperatures increase about 30% reaching values as high as 320°C. The estimated separation distances in Figure 4.11b also points out to the improvement: the reaction regions propagate coherently with an average distance of 1 meter at air injection rates as low as 100 m/day. The coherent propagation velocity of the reaction regions decreases in Figure 4.11c, however insignificantly.

Interestingly, two local regions of air injection rates exist where the separation distance is either infinitely large, i.e., $\xi^* \to \infty$, (near 100 m/day) or infinitesimally small, i.e., $\xi^* \to 0$, (at extremely low injection rates); namely, at these injection rates, the reaction regions do not cohere, thus, become either fully separated from or overlap each other. For those injection rates, no real solutions to the coupled algebraic equations exist. Hence, the model of combustion front propagation with sequential reactions yields an upper and lower air injection limits emphasizing two possibilities of combustion failure in the reservoir other than reaction extinction. Nevertheless, in between these limits, coherent combustion front propagation is predicted.

It is also found that dual effects have a preferential dominance on the combustion front behavior. The catalytic effects play a role on improvement of the combustion performance at low air injection rates, where, under the influence of reservoir heat losses, the HTO temperature drops significantly; on the other hand, the fuel deposition effect is more pronounced on the combustion performance at high air injection rates.

Regardless of their preferential influences, the combustion front propagates at relatively low temperatures and velocities as the air injection rate (reservoir heat losses) is decreased (increased). Note in Figure 4.11a that the front appears not to be influenced significantly by the presence of dual effects at injection rates less than 100 m/day. Disappointingly, in this region, the temperature drop is so large and overall influence of the catalytic agents is so small that the front is expected to have no significant impact on recovery under the deleterious reservoir conditions. Important issues need to be addressed for application of air injection methods are then identification of the optimum reservoir conditions and selection of suitable catalytic agents that could prevent these observed drastic temperature drops.

Indeed, a better understanding of dual effects under reservoir conditions is required which calls for a detailed analysis using the described combustion front propagation model in the complete parameter space. The task, however, is a rather challenging one, since the problem is large (due to number of parameters varying in the presence of catalytic agents) and involves nonlinearities inherent to the oxidation reactions, their interactions. A three-step approach is used to analyze and optimize the combustion front dynamics.

HTO Fuel Generation Efficiency As a first step, for an optimum HTO fuel generation efficiency that could lead to a high-performance front propagation is investigated. This requires analysis of unique solutions to equations (10-11) and (17-18) with the base-state values in a two-dimensional space of HTO and LTO fuel densities ρ^o_{fH}, ρ^o_{fL}. The interest is to determine where, in the fuel generation efficiency space, the estimated HTO temperature, front propagation velocity and oxygen consumption efficiency are the

highest as the separation distances of the reaction regions remain finite, e.g., in the order of 10 cm. Figure 4.12 shows distribution of the solutions when fuel densities are increased in the range % 0-100. It is clear that a large region of the space does not contain solutions corresponding to the state of frontal coherence: the reaction regions are fully separated when the HTO fuel density change is % 35 or higher. For changes less, coherent front propagation is predicted, however. In this region, the propagation velocity and oxygen consumption efficiency increases with the hydrocarbon deposition ahead of the front. It appears that the HTO front temperature also increases, however not significantly.

These observations emphasize the importance of LTO reaction stoichiometry. Fractions of the total amount of hydrocarbons used by the reactions appear to play a significant role on the frontal coherence and on the combustion performance.

Dual Effects In the second step, solutions in another two-dimensional parameter space are investigated. Here, x-y coordinates of the space correspond to the combined kinetic effects and to the fuel deposition effect of the catalytic agents, respectively. They reflect the per cent change in the kinetic and fuel deposition parameters. For example, the front propagation solution obtained at point (x=0.4, y=0.6) in the dual effect space is that particular solution for which the activation energies and frequency factors of the HTO and LTO reactions are changed % 40 from their base-values, the specific fuel surface areas are changed % 40, whereas the fuel densities are increased % 60. Note that, in this part of the analysis, the fuel densities are increased with the same proportion so that the effective stoichiometric coefficient of the LTO, hence, the fuel generation efficiency does not change.

Figure 4.13 shows that frontal coherence exists for a large central portion of the dual effect space. Outside of the region of coherence the HTO and LTO reaction regions are either fully separated from or overlap each other. Next, an optimum point inside the coherence area that could lead the combustion front propagation to maximum performance is searched. The interest is to determine where, in the region of coherence,

the estimated HTO temperature and propagation velocity values are the highest and the separation distance is finite. The distance is typically 50-150 cm; its values increase abruptly close to the boundary of frontal separation, however. As the kinetic and fuel deposition effects increase proportionally, the front maintains larger temperature and velocities, its oxygen consumption efficiency increases. There exist a clear and smooth gradation on the values of the latter properties in the SW-NE direction until roughly (x=0.35, y=0.35) point is reached in the region of coherence; at larger values, however, nonlinearities appear, in particular, in the case of propagation velocity. Consequently, no localized area in the region of coherence gives solutions that lead to ideal combustion performance. The front can reach extremely high temperatures, consuming nearly all of the injected oxygen but, it has to compromise on its propagation speed and travel throughout the reservoir at relatively lower speeds. Consider, for example, the case where catalytic agents led to a % 80 or higher increase in the kinetic and fuel deposition effects. The improvement on the HTO temperature and oxygen consumption efficiency is significant. The temperature now reaches values as high as 600-650°C in the presence of reservoir heat losses; whereas the front propagation in the reservoir stays in the range of 2.4-3.0 m/day.

As final step, front propagation when a catalytic agent creates reservoir conditions that satisfy an optimal case is investigated in the complete parameter space. Figure 4.14 shows the estimated results when the HTO and LTO fuel densities are increased % 10 and % 90 respectively, as the kinetic and fuel deposition parameters are changed % 80 and % 50. The figure also compares these results with the base case of Figure 4.11 in the absence of catalytic agents. Note the significant improvement on the temperatures of HTO and LTO reaction regions. The combustion front now maintains a maximum temperature above 500°C for a large range of injection velocities. The maximum temperature drop still persists at low rates; however, the temperature values in this range are 400°C or higher. The possibility of combustion process failure due to separation of the reaction regions does not appear to be an issue of significant importance, since the estimated separation distances are less than one meter and vary in the order of 10 cm. At extremely low injection rates, less than 20 m/day, a possibility for reaction regions to

overlap each other still exists, however. Due to selected optimum values, the coherent front propagation velocity is estimated to be less than the base case; regardless, it varies in a reasonable range (0.5-3.8 m/day) for the considered air injection rates.

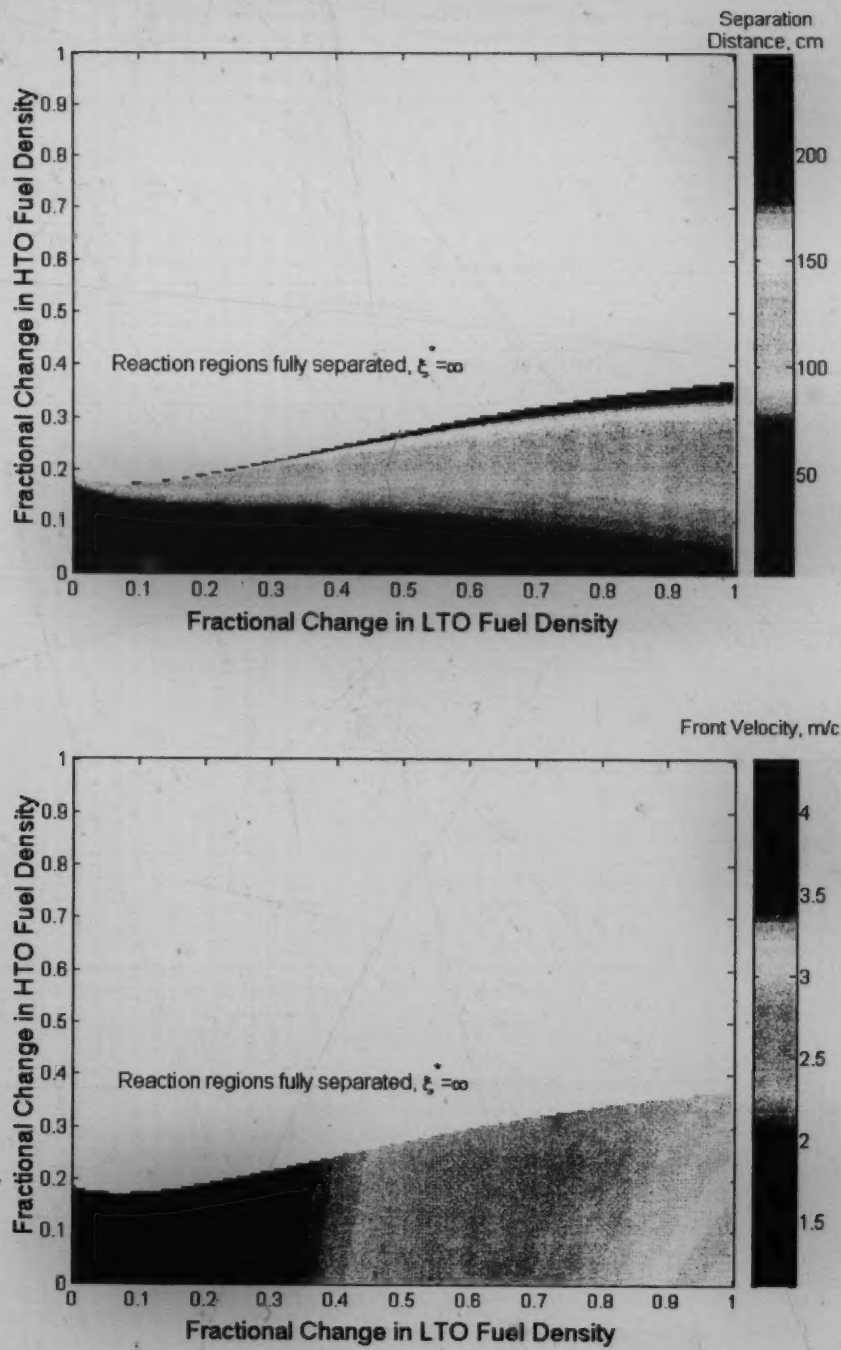

Figure 12 a - Separation distance (upper) and coherent front propagation velocity (lower) of the reaction regions in the HTO fuel generation space. (x, y) coordinates are (ρ^o_{fL}, ρ^o_{fH}), injection velocity is 300 m/day.

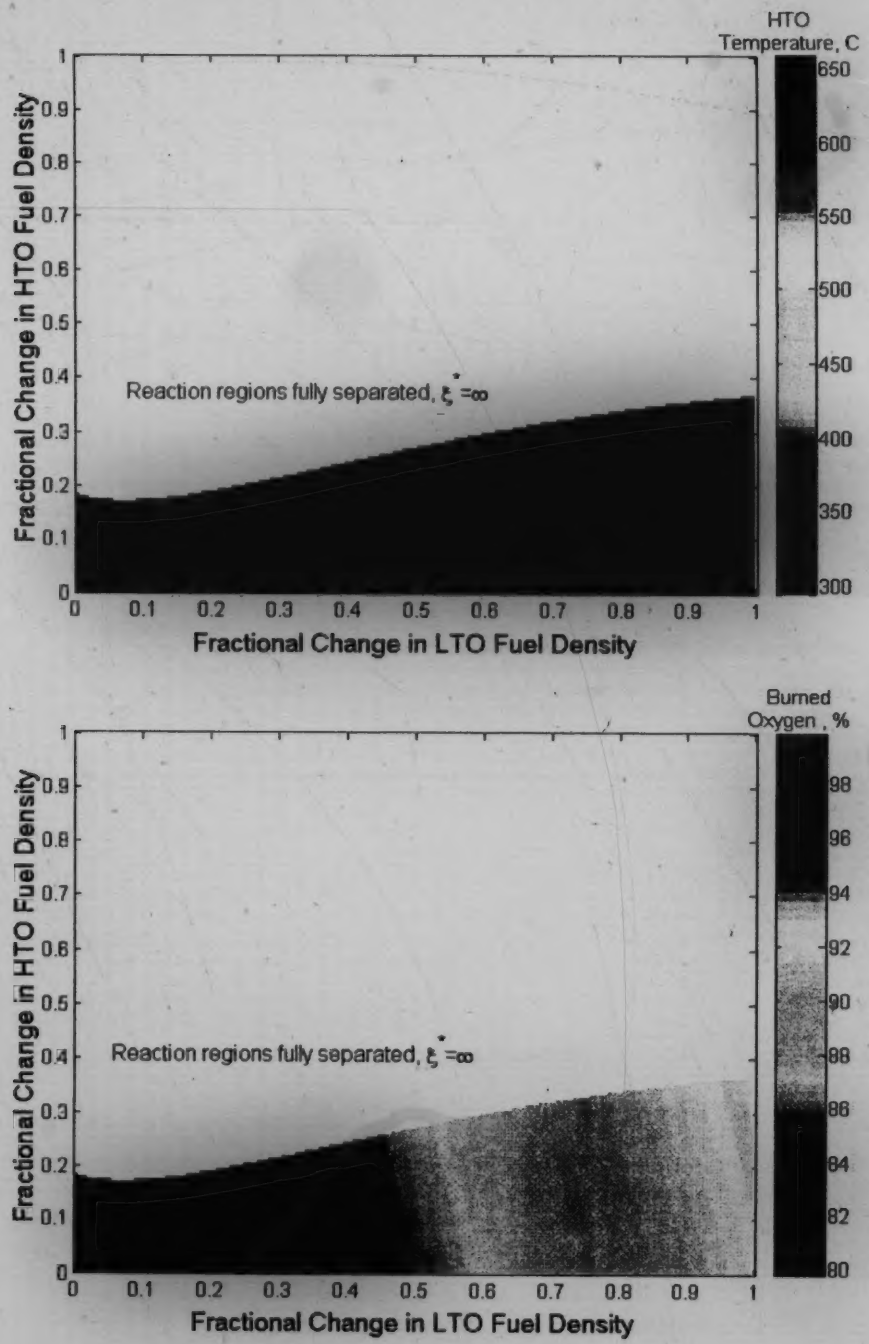

Figure 12 b-HTO temperature (upper) and oxygen burning efficiency (lower) of the combustion front in the HTO fuel generation space. (x, y) coordinates are (ρ^o_{fL}, ρ^o_{fH}), injection velocity is 300 m/day.

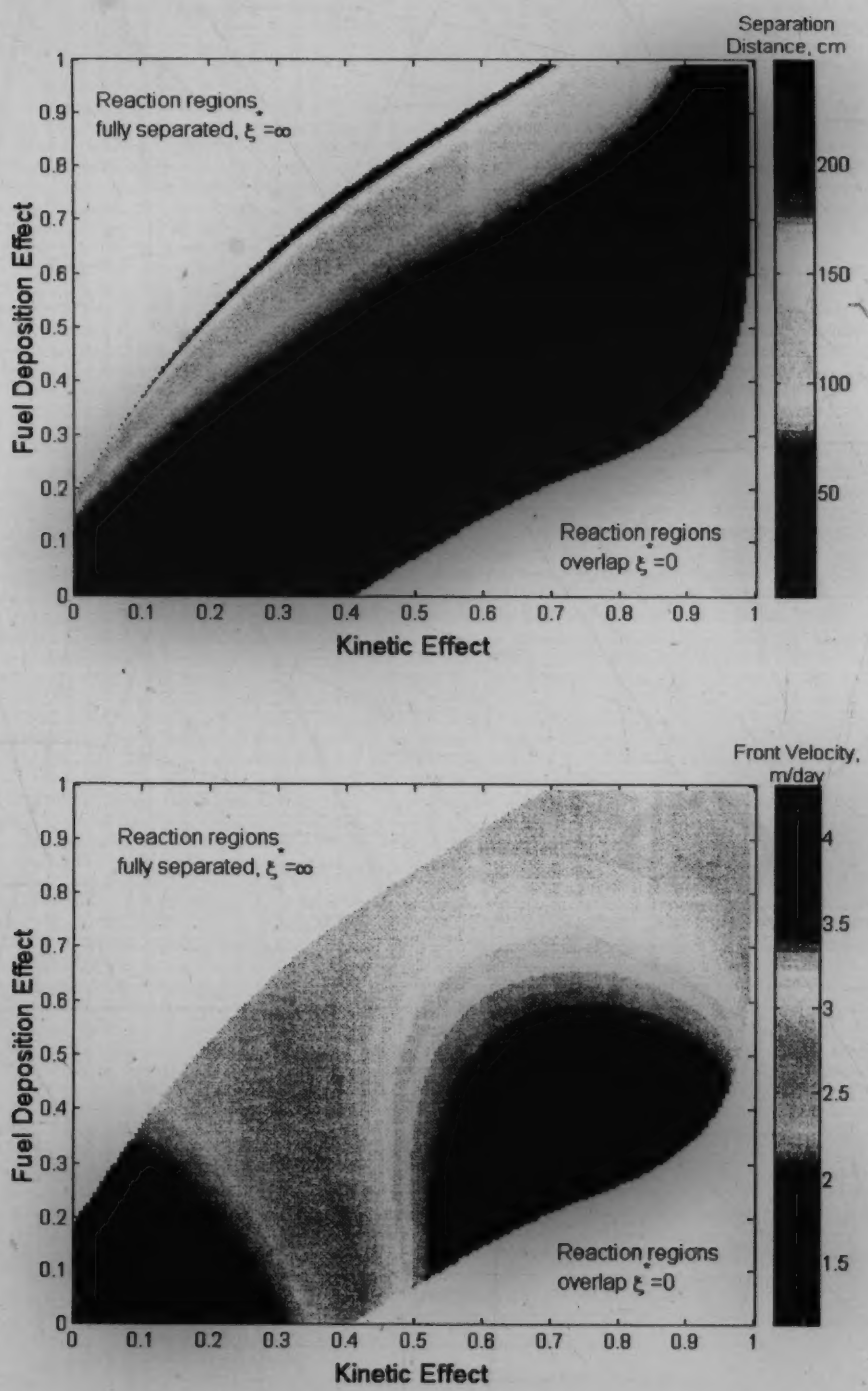

Figure 13 a - Separation distance (upper) and coherent front propagation velocity (lower) of the reaction regions in the space of dual effects. Injection velocity is 300 m/day.

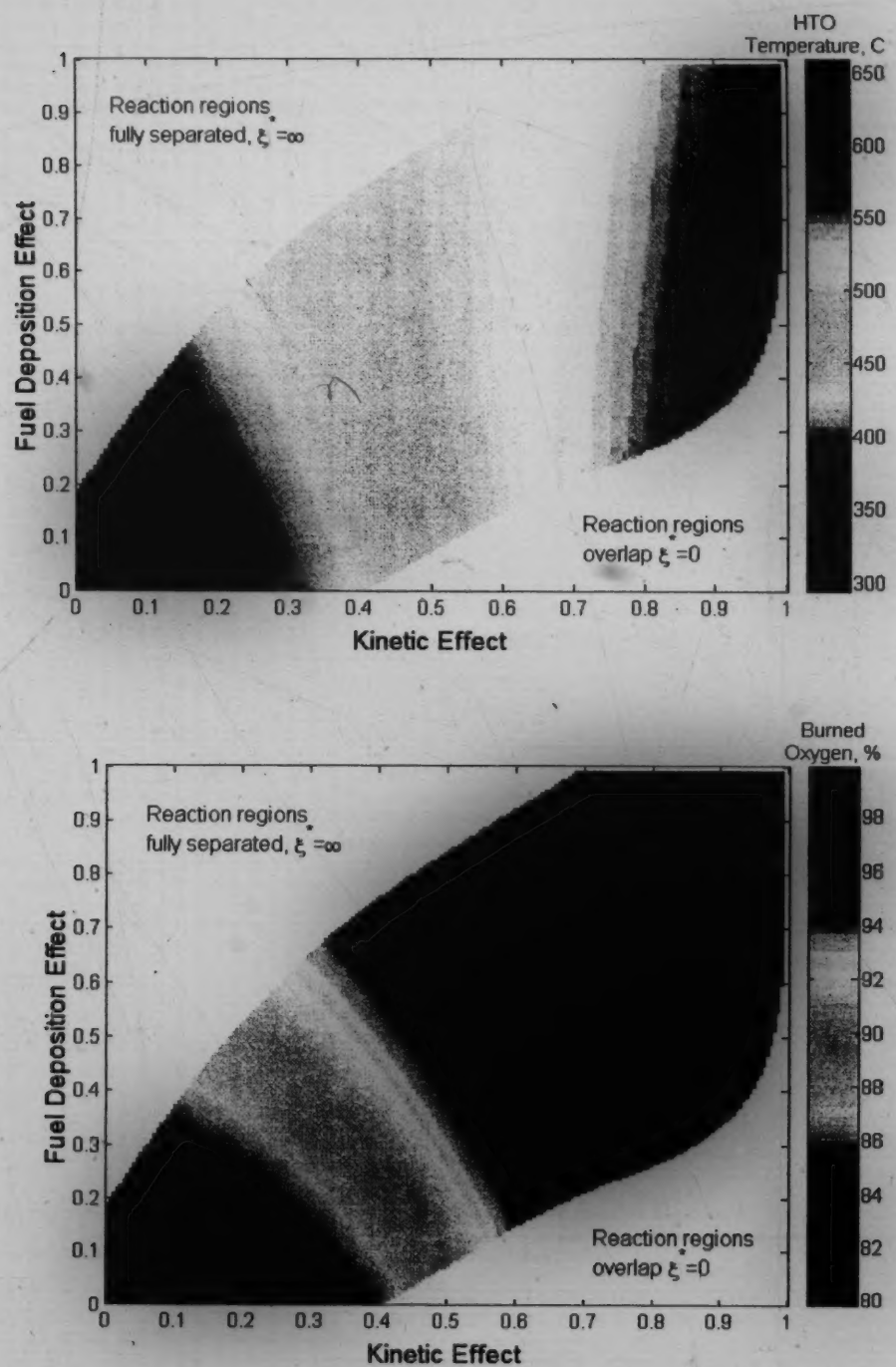

Figure 13 b - HTO temperature (upper) and oxygen burning efficiency (lower) of the combustion front in the space of dual effects. Injection velocity is 300 m/day.

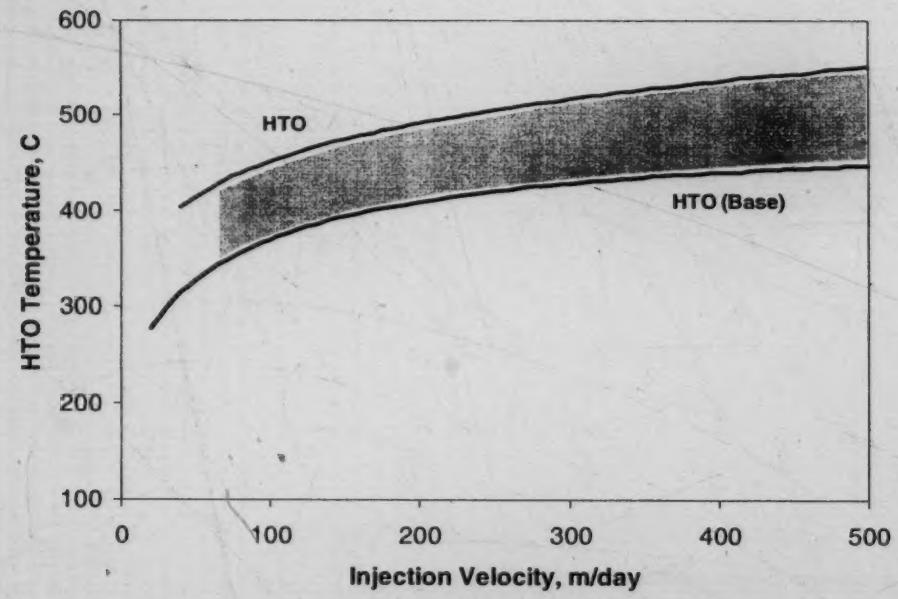

Figure 14 a - Comparison of the combustion HTO front temperature under the optimal influence of catalytic agents with the base-state solution of Figure 4.13

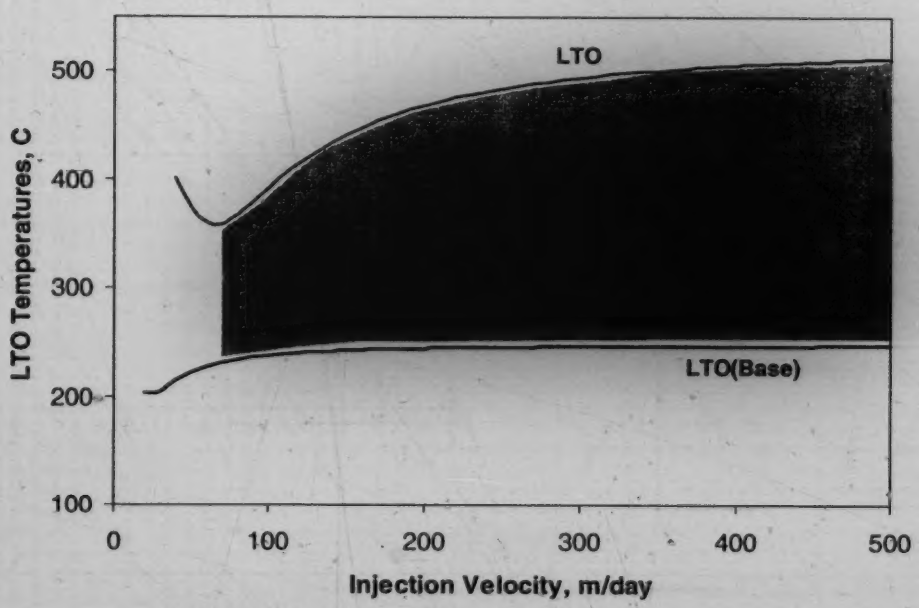

Figure 14 b - Comparison of the combustion LTO front temperature under the optimal influence of catalytic agents with the base-state solution of Figure 4.13

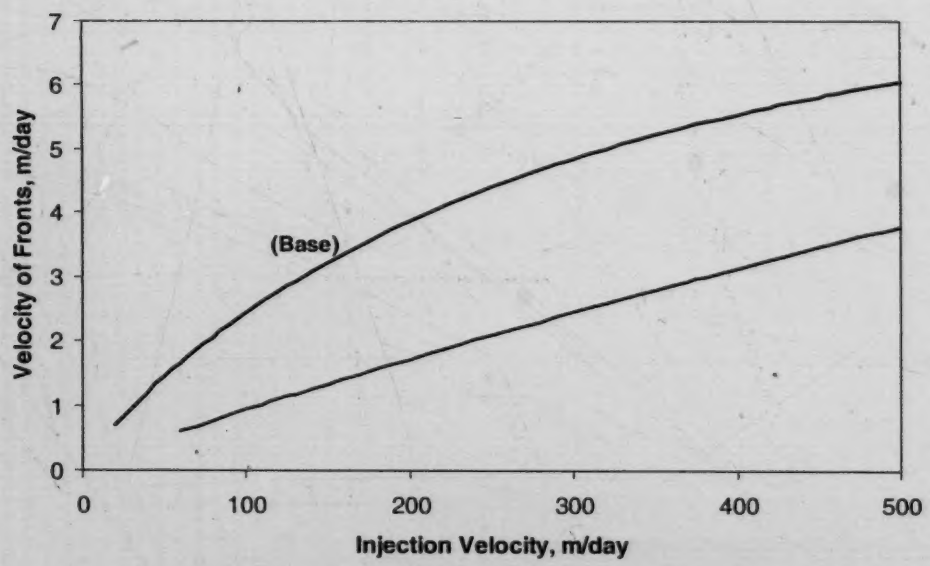

Figure 14 c - Comparison of the combustion front velocity under the optimal influence of catalytic agents with the base-state solution of Figure 4.13

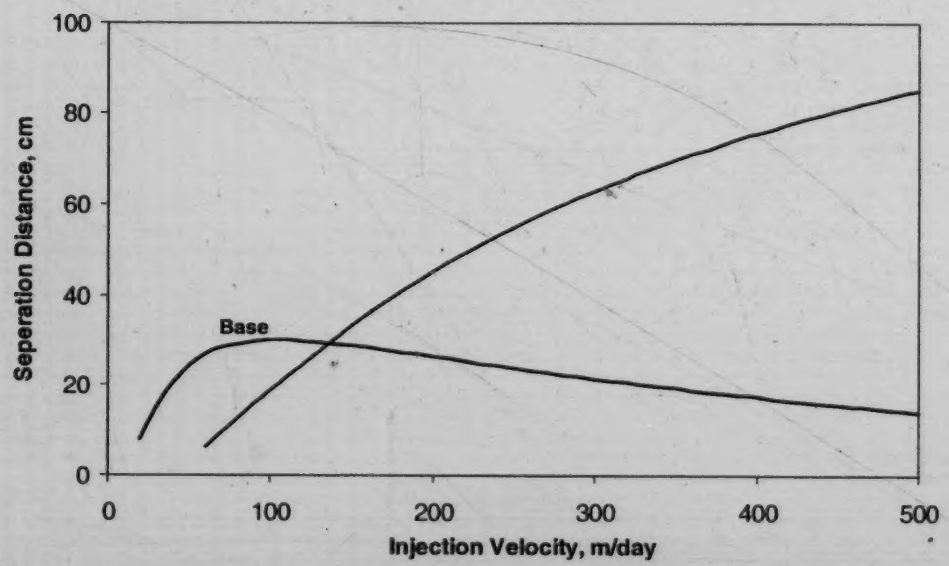

Figure 14 d - Comparison of the separation distance of the fronts under the optimal influence of catalytic agents with the base-state solution of Figure 4.13 in the absence of catalytic agents. E_H=13.2 E4 kJ/kmole , E_L=1.9 E4 kJ/kmole , a_{sH}=2.8 E4 m^2/m^3, a_{sL}=2.5 E5 m^2/m^3, k_H=1.4 E6 kW-m/atm-kmole, k_L=0.0694 kW-m/atm-kmole, ρ^o_{fH} =18.81 kg/m^3, ρ^o_{fL} = 43.32 kg/m^3.

CHAPTER 5

CONCLUSIONS AND RECOMMENDATIONS

In-situ combustion front propagation involves diffusive processes and complex chemical reactions. Traditional approach to analysis of the combustion fronts is based on classification of the crude oils according to their oxidation characteristics. At least two distinct temperature ranges, HTO and LTO, have been found to affect the propagation characteristics. Properties and interaction of these two distinct reaction regions were investigated using an analytical approach. Reaction regions have a spatially narrow width within which heat release, and reaction rates vary significantly. The narrow width calls for an approach in which these reaction regions are treated as surface of discontinuities in the appropriate variables. The models developed reduce the complex nonlinear problem of combustion front propagation with a fuel generating reaction to a system of coupled algebraic equations.

The reaction regions could self-sustain and propagate in the reservoir within a distance from each other that could vary significantly. Under the adiabatic conditions, there exist two limits to the propagation: the fronts could either coincide (with a distance nil); or they could become infinitely separated and de-coupled. The extent of these limits in the injection velocity space varies significantly with the kinetics and stoichiometry of the fuel generating reaction.

In the presence of external heat losses, although coherent propagation takes place within a much larger portion of the same parameter space, the combustion front propagates at lower temperatures and velocities. It is found out that the reactions regions of a combustion front have the ability to travel closely spaced and, consequently, minimize

the effects of reservoir heat losses. This mechanism is shown to thermally support the combustion front under deleterious reservoir conditions.

Dual (catalytic/fuel deposition) effects of clays, metallic minerals and additives on coherent propagation of the HTO and LTO reaction regions are investigated. It is found that the reservoir heat losses are detrimental to in-situ combustion process: at low air injection rates, temperature of the combustion front drops drastically. In the presence of clays/additives, this deleterious influence of heat losses persists. The presence, however, may have a significant impact on the combustion front performance at high injection rates.

A contrast in the activation energies of the oxidation reactions improved the combustion performance. A normal compensation effect, however, eliminated this improvement. According to the formulation of the model, in the presence of the latter, a positive catalytic effect appears to be possible only if the reaction rates change due to variations in the specific surface areas of the hydrocarbon fuels. In the literature, often the product ka_s is considered the frequency factor. If the compensation effect is due to *k-E* relationship only and excludes the variations in the fuel surface area, then the combustion process could be enhanced by the variations in specific fuel surface areas.

Investigation regarding fuel densities showed that hydrocarbon deposition markedly influences the LTO region temperature: the LTO temperature could become comparable and even higher than the HTO region temperature as the hydrocarbon deposition increases ahead. A significant improvement on the overall combustion performance is possible, however, only when the HTO fuel is generated in direct proportions to the hydrocarbon deposition ahead of the LTO region. The latter points out the significance of HTO fuel generation stoichiometry on the in-situ combustion dynamics. When the HTO fuel generation is favorable and in particular at high (low) air injection (heat loss) rates, a strong combustion enhancement effect could be observed in the presence of clays, metallic minerals and additives, due to the role they play in modifying specific surface area of the solid grains and, hence, on deposition of the hydrocarbons.

The results emphasize the importance of reservoir selection prior to any air injection and in-situ combustion process and calls for a consideration and discreet screening of the catalytic agents with the purpose of increased control over the in-situ combustion front propagation.

REFERENCES

1. Akkutlu, I.Y., and Yortsos, Y.C.: "Dynamics of Combustion Fronts in Porous Media" paper SPE 63225, presented at the SPE Annual Tec. Conf. and Exhibit, Dallas TX (Oct. 1-4, 2000).

2. Akkutlu, I.Y., and Yortsos, Y.C.: "The Dynamics of In-situ Combustion Fronts in Porous Media" *Combustion and Flame* 134 (2003) 229-247.

3. Akkutlu, I.Y., and Yortsos, Y.C.: "Steady-State Propagation of In-situ Combustion Fronts with Sequential Reactions" paper SPE 91957, presented at the SPE Int. Petroleum Conference, held in Puebla Mexico (Nov 8-9, 2004).

4. Alexander, J.D., Martin, W.L., and Dew, J.N.: "Factors Affecting Fuel Availability and Composition During In-Situ Combustion," *J. Pet. Tech.* (Oct. 1962) 1154-1164.

5. Bae, J.H.: "Characterization of Crude Oil for Fireflooding Using Thermal Analysis Methods" *Soc. of Pet. Eng. J.* (June 1977) 211-217.

6. Beckers, H.L. and Harmsen, G.J.: "The Effect of Water Injection on Sustained Combustion in a Porous Medium" *Soc. of Pet. Eng. J.* (June 1970) 145-163.

7. Benham, A.L. and Poettmann, F.H.: "The Thermal Recovery Process-An Analysis of Laboratory Combustion Data," *Trans., AIME* 213 (1958) 406-408.

8. Britten, J.A. and Krantz, W.B.: "Asymptotic Structure of Planar Nonadiabatic Reverse Combustion Fronts in Porous Media," *Combustion and Flame,* 65 (1986) 151-161.

9. Burger, J.G. and Sahuquet, BC.: "Chemical Aspects of In-Situ Combustion – Heat of Combustion and Kinetics" *Soc. of Pet. Eng. J* (Oct. 1972) 410-422.

10. Castanier, L. M., Baena, C. J., Tavares, C., Holt, R. J., and Brigham, W. E.: "In Situ Combustion with Metallic Additives" paper SPE 23708, presented at the SPE-AIME Latin American Petroleum Engineering Conference, Caracas (March 1992).

11. Dabbous, M.K. and Fulton, P.F.: "Low-Temperature Oxidation Reaction Kinetics and Effects on the In-Situ Combustion Process," *Soc. of Pet. Eng. J.* (June 1974) 253-262.

12. De Los Rios, C. F., Brigham, W. E., and Castanier, L. M.: "The Effect of Metallic Additives on the Kinetics of Oil Oxidation Reactions in In-Situ Combustion"

Stanford University Petroleum Research Institute, SUPRI-TR-63, Report submitted to the U.S. Dept. of Energy under contract no. DEFG19-87BC14126, Stanford University, Stanford, California (November 1988).

13. Dietz, D.N. and Weijdema, J: "Wet and Partially Quenched Combustion" *J. Pet. Tech.* (April 1963) 411-415.

14. Drici, O. and Vossoughi, S.: "Study of the Surface Area Effect on Crude Oil Combustion by Thermal Analysis Techniques" *J. Pet. Tech.* 37 (April 1985) 731-735.

15. Fassihi, M.R.: "Analysis of Fuel Oxidation in In-situ Combustion Oil Recovery" PhD dissertation, Stanford University, Stanford, CA (May 1981).

16. Greaves, M. and Al-Shamali, O.: "In situ combustion (ISC) process using horizontal wells" *J Can Pet Tech.*, 35(4) (1996) 49–55.

17. Greaves, M. and Al-Shamali, O.: "Wet in situ combustion (ISC) process using horizontal wells" Proceedings 6th UNITAR International Conference on Heavy Oil and Tar Sands, Houston, Texas (1995) 90–112.

18. Greaves, M. and Turta, A.: "Oil Field In-situ Combustion Process" United States Patent no. 5, 626, 191 (May 6, 1997)

19. Greaves, M., Tuwil, A.A. and Bagci, A.S.: "Horizontal Producer Wells In-situ Combustion (ISC) Processes" *J Can Pet Tech.*, 32(4) (1993) 58–67.

20. He, B., Chen, Q., Castanier, L.M. and Kovscek A.R.: "Improved In-Situ Combustion Performance With Metallic Salt Additives" paper SPE 93901, presented at SPE Western Regional Meeting, Irvine, CA (March 30 – April 1, 2005)

21. Holt R. J.:"In Situ Combustion with Metallic Additives" SUPRI TR. 87, Stanford University (July 1992).

22. Kisman, K.E. and Lau, E.C.: "A new combustion process utilizing horizontal wells and gravity drainage" The CIM Annual Technical Conference, Calgary (May 9-12, 1993).

23. Kok, M.V., and Karacan, C.O.: "Behaviour and Effect of SARA Fractions of Oil during Combustion" SPE Reservoir Evaluation and Engineering, Vol. 3, No. 5 (October 2000) 380-85.

24. Mamora, D. D.: "Kinetics of In-Situ Combustion" Ph.D. dissertation, Stanford U., Stanford, CA (May 1993)

25. Moore, R.G., Bennion, D.W., Millour, J.P., Ursenbach, M.G., and Crie, D.N.: "Comparison of the Effect of Thermal Cracking and Low Temperature Oxidation on Fuel Deposition During In-Situ Combustion" Proceedings of the Tar Sands Symposium, Jackson, Wyoming U.S. DOE Report, DOE/METC-87/6073 (CONF-860717) (July 7–10, 1986) 270-283.

26. Moritis, G.: "Biennial EOR Production Report-California Steam EOR Produces less, other EOR Continues" *Oil and Gas Journal* (April 15, 2002) 72.

27. Parrish, D.R. and Craig, F.F.: "Laboratory Study of a Combination of Forward Combustion and Waterflooding-The COFCAW Process" *J. Pet. Tech.* (June 1969) 753-761.

28. Poettmann F.H., Schilson, R.E. and Surkalo, H.: "Philosophy and Technology of In-Situ Combustion in Light Oil Reservoirs" Proc. of the Seventh World Pet. Cong., Mexico City (1967) 111 - 487.

29. Prats, M. *Thermal Recovery,* SPE Monograph series (1982)

30. Sarathi P.S.: "In-situ Combustion Handbook-Principles and Practices" final report, BDM Petroleum Technologies, contract No.DE-AC22-94PC91008, Bartlesville, Oklahoma (November 1998).

31. Shallcross, D. C., de los Rios, C.F., Castanier, L.M., and Brigham, W.E.: "Modifying In Situ Combustion Performance by the use of Water-Soluble Metallic Additives" paper SPE 19485, presented at the SPE AIME Asia-Pacific Conference, Sydney, Australia (September 13-15, 1989).

32. Showalter, W.E.: "Combustion Drive Tests" *Soc. of Pet. Eng. J.* (March 1963) 53-58.

33. Vossoughi, S., Willlhite, G.P., Kritikos, W.P., Guvenir, I.M., and El Shoubary, Y.: "Automation of an In-Situ combustion Tube and Study of the Effect of Clay on the In-Situ combustion Process" *Soc. of Pet. Eng. J.* (Aug. 1982) 493-502.

34. Williams, F.A. *Combustion Theory* Benjamin and Cummings Publishing Company Inc. (1985).

APPENDIX A

Calibration of Two-reaction Combustion Front Propagation

Two-reaction combustion front propagation is calibrated and become comparable to the results of single-reaction front problem by always keeping the total heat content of the reservoir the same: $q_H + q_L = q$. In terms of the dimensional quantities this equality can be written as the following:

$$Q_H \rho^o_{fH} + Q_L \rho^o_{fL} = Q \rho^o_f \tag{A1}$$

which is also equal to:

$$\left(\frac{Q_H}{Q}\right)\left(\frac{\rho^o_{fH}}{\rho^o_f}\right) + \left(\frac{Q_L}{Q}\right)\left(\frac{\rho^o_{fL}}{\rho^o_f}\right) = 1.0 \tag{A2}$$

By taking $Q=Q_H$, and defining $R_Q=Q_L / Q_H$, we get:

$$\left(\frac{\rho^o_{fH}}{\rho^o_f}\right) + R_Q\left(\frac{\rho^o_{fL}}{\rho^o_{fH}} \times \frac{\rho^o_{fH}}{\rho^o_f}\right) = 1.0 \tag{A3}$$

Now, we define a new parameter $\alpha=\rho^o_{fH}/\rho^o_f$, along with $R_F=\rho^o_{fL}/\rho^o_{fH}$. Then, in a compact form we get:

$$\alpha + R_Q(\alpha R_F) = 1.0 \tag{A4}$$

If we re-organize this equation, we obtain the condition necessary to keep the two-reaction combustion front thermally comparable to the single-reaction front:

$$R_F = \frac{1}{R_Q}\left(\frac{1}{\alpha} - 1\right) \qquad \text{(A5)}$$

APPENDIX B

The code for Nonadiabatic Steady State Solutions for Sequential Reaction Fronts

```
% Nonadiabatic Steady State Solutions for Sequential Reaction Fronts
% Derya Adagulu, University of Alberta
% Last Updated March, 2006
%
 clear all
%
% Enter Parameters for HTO rxn
% EH=7.352E+4*1.05;     % kJ/kmole
QH=3.9542E+4;    % kJ/kg
% kH=227.0*1.27;        % kW-m/atm-kmole
tilmuH=3.018;    % dimensionless
tilmugH=1.0;     % dimensionless
%
% Enter Parameters for LTO
% EL=0.715*EH*0.95;      % kJ/kmole
QL=0.5*QH;       % kJ/kg
% kL=227.0*0.79;        % kW-m/atm-kmole
tilmuL=3.018;    % dimensionless
tilmugL=1.0;     % dimensionless
%
% Enter Common Parameters
H=0.5;             % m
tildeh=0.078;      % kW/m^2-K
alpha_s=4.3E-7;    % m^2/s
To=373.15;         % K
Yi=0.23;           % kg/kg
capacity=2.012E+3;% kJ/m^3-K

p=10.0;            % atm
R=8.314;           % kJ/kmole-K
%
 %Calculate the Calibrated fuel densities for HTO and LTO
%  alpha=0.6;
%  RQ=QL/QH;
%  RF=1/RQ*(1/alpha-1);

% rho_fH=19.0*alpha
% rho_fL=RF*rho_fH

vi_mday=300;% m  /day

rho_x=0.90:0.001:0.995;
```

```
for k=1:length(rho_x);

rho_fH(k)=11.4+11.4*rho_x(k);
rho_fL(k)=15.2+15.2*rho_x(k);

kin_x=0.00:0.005:0.995;
for z=1:length(kin_x);

aaa=rho_x(k)
bbb=kin_x(z)

EH(z)=7.352E+4 + 7.352E+4*kin_x(z);    % kJ/kmole
%  kH(z)=227.0 ;    % kW-m/atm-kmole
EL(z)=0.715*EH (z)- 0.715*EH(z)*kin_x(z);    % kJ/kmole
%  kL(z)=227.0  ;   % kW-m/atm-kmole

logkh(z)=(6.453E-5*EH(z))-2.38;
kH(z)=10^logkh(z);
logkl(z)=(6.453E-5*EL(z))-2.38;
kL(z)=10^logkl(z);
%
% asH(z)=1.41E+5 + 1.41E+5*kin_x(z)      % m^2/m^3
% asL(z)=1.41E+5 - 1.41E+5*kin_x(z)

asH(z)=1.41E+5-1.41E+5*kin_x(z);   % m^2/m^3
asL(z)=1.41E+5+1.41E+5*kin_x(z);

%
% Calculate rho_gi, qH, qL, gammaH, gammaL, muH, mugH

qH=QH*rho_fH(k)/(capacity*To);
qL=QL*rho_fL(k)/(capacity*To);
gammaH=EH(z)/(R*To);
gammaL=EL(z)/(R*To);

%rho_gi=p*1.01325E+5*29/(8.314*1000*To);
%muH=tilmuH*rho_fH/(rho_gi*Yi);
%mugH=tilmugH*rho_fH/rho_gi;
%
% Set Air Injection Velocity Range for Calculations
% vi_mday=25.0
vi=vi_mday/(24*3600);
%vi_mday=100:100:1000;       % m/day
%for i=1:length(vi_mday);
%    vel=vi_mday(i)
%    vi=vi_mday(i)/(24*3600);
    % Calculate dimensionless heat loss coefficient, h
    l_star=alpha_s/vi;    % meter
    t_star=alpha_s/vi^2;
    h=tildeh*t_star/(capacity*H);
    %
    % Calculate calAH
    calAH=asH(z)*alpha_s*kH(z)*p*Yi/(qH*EH(z)*vi^2);
    %
    % Guess HTO Front Temperature
```

```
T_fH=272:0.01:600;          % Celsius
for j=1:length(T_fH);
    TfH(j)=T_fH(j)+273.15;  % Kelvin
    rho_gi=p*1.01325E+5*29/(8.314*1000*T_fH(j));
    muH=tilmuH*rho_fH(k)/(rho_gi*Yi);
    mugH=tilmugH*rho_fH(k)/rho_gi;
    thetafH=TfH(j)/To;
    %
    % Calculate Roots of Cubic VDH Equation
    betaH=calAH*thetafH*exp(-gammaH/thetafH);
    pH=[mugH 1 muH*betaH -betaH];
    rt_H=roots(pH);
    %
    % Determine Positive Real Root of VDH
    if rt_H(1)>0;
        rt_H(2)<0;
        rt_H(3)<0;
        VDH=rt_H(1);
    else
        if rt_H(2)>0;
            rt_H(1)<0;
            rt_H(3)<0;
            VDH=rt_H(2);
        else
            if rt_H(3)>0;
                rt_H(1)<0;
                rt_H(2)<0;
                VDH=rt_H(3);
            end
        end
    end
    %
    % Calculate Normalized Unburned Oxygen Mass Fraction Ahead of
HTO Front

    YH=(1-muH*VDH)/(1+mugH*VDH);
    %
    % Calculate calAL, muL, mugL
    calAL=asL(z)*alpha_s*kL(z)*p*YH*Yi/(qL*EL(z)*vi^2);
    muL=tilmuL*rho_fL(k)/(rho_gi*YH*Yi);
    mugL=tilmugL*rho_fL(k)/rho_gi;
    %
    % Calculate the Nondimensional Separation Distance
    Delh=sqrt(1+4*h/VDH^2);



    lhs=-2.0*log((thetafH-1-qH/Delh)*Delh/qL);

    xi_star=lhs/((Delh-1.0)*VDH);
    %
    % Calculate theta_fL

    thetafL=1+(qL/Delh)+(qH/Delh)*exp(-0.5*(Delh+1)*VDH*xi_star);
```

```
%
% Calculate Roots of Cubic VDL Equation
betaL=calAL*thetafL*exp(-gammaL/thetafL);
pL=[mugL 1 muL*betaL -betaL];
rt_L=roots(pL);
%
% Determine Positive Real Root of VDL
if rt_L(1)>0;
    rt_L(2)<0;
    rt_L(3)<0;
    VDL=rt_L(1);
else
    if rt_L(2)>0;
        rt_L(1)<0;
        rt_L(3)<0;
        VDL=rt_L(2);
    else
        if rt_L(3)>0;
            rt_L(1)<0;
            rt_L(2)<0;
            VDL=rt_L(3);
        end
    end
end
%
% Compare the Estimated Front Propagation Velocities
VH=VDH*vi_mday;
VL=VDL*vi_mday;
if  abs(VH-VL)<10^-2;
%       display('Convergence is ok');
%
%Calculate Normalized Unburned Oxygen Mass Fraction Ahead of LTO Front
%
        CORR=((thetafH-1-qH/Delh)*Delh/qL);

        if CORR<0 | xi_star<0;

            SD(k,z)=NaN;
            YL(k,z)=NaN;
            YHX(k,z)=NaN;
            YLX(k,z)=NaN;
            VLX(k,z)=NaN;
            VHX(k,z)=NaN;
            TFHX(k,z)=NaN;
            TFLX(k,z)=NaN;
        else

         YL(k,z)=(1-muL*VDL)/(1+mugL*VDL);
         SD(k,z)=xi_star*l_star*100.0;

         YHX(k,z)=YH*Yi;
         YLX(k,z)=YL(k,z)*YH*Yi;

         VHX(k,z)=VH;
         VLX(k,z)=VL;
```

```
            TFHX(k,z)=thetafH*To-273.15
            TFLX(k,z)=thetafL*To-273.15;
            break
          end

      end

end
end
end

yy=rho_x;
xx=kin_x;
          [xx,yy]=meshgrid(xx,yy);
          zz=TFHX;
          pcolor(xx,yy,zz),colorbar;
          colormap jet
          shading interp
          axis([0 1 0 1 ]);
          xlabel('Kinetic Effect','Fontsize',14,'Rotation',0);
          ylabel('Fuel Deposition Effect','Fontsize',14,'Rotation',90);
          text(0.2,0.8,' Reaction regions fully separated,
\xi^{*}=\infty','FontSize',14)
          text(0.8,0.1,' Reaction regions overlap
\xi^{*}=0','FontSize',14)
          hcb = colorbar('horiz')
          set(get(hcb,'Title'),'String','HTO Temperature';',
C','FontSize',12)
%           hold on
%           [c,h]=contour(xx,yy,zz);
%           contour(xx,yy,zz,50,'k');
%
%           clabel(c,h,'FontSize',17,'Color','k','Rotation',0);
%           hold off
%           zlabel('HTO Temperature,C')
%
%           zlabel('Seperation Distance,cm')
%           zlabel('Front Velocity,m/day')

%end
```